R.R.C.
8-10-82

Advanced Gas Turbine

DOE/NASA/0168-82/4
NASA CR-167875
DDA EDR 10977

AGT

Power-Train System Development

Fourth Semiannual Report
For work performed from 1 July 1981 - 31 December 1981

Detroit Diesel Allison
Division of General Motors Corporation
Indianapolis, Indiana 46206

February 1982

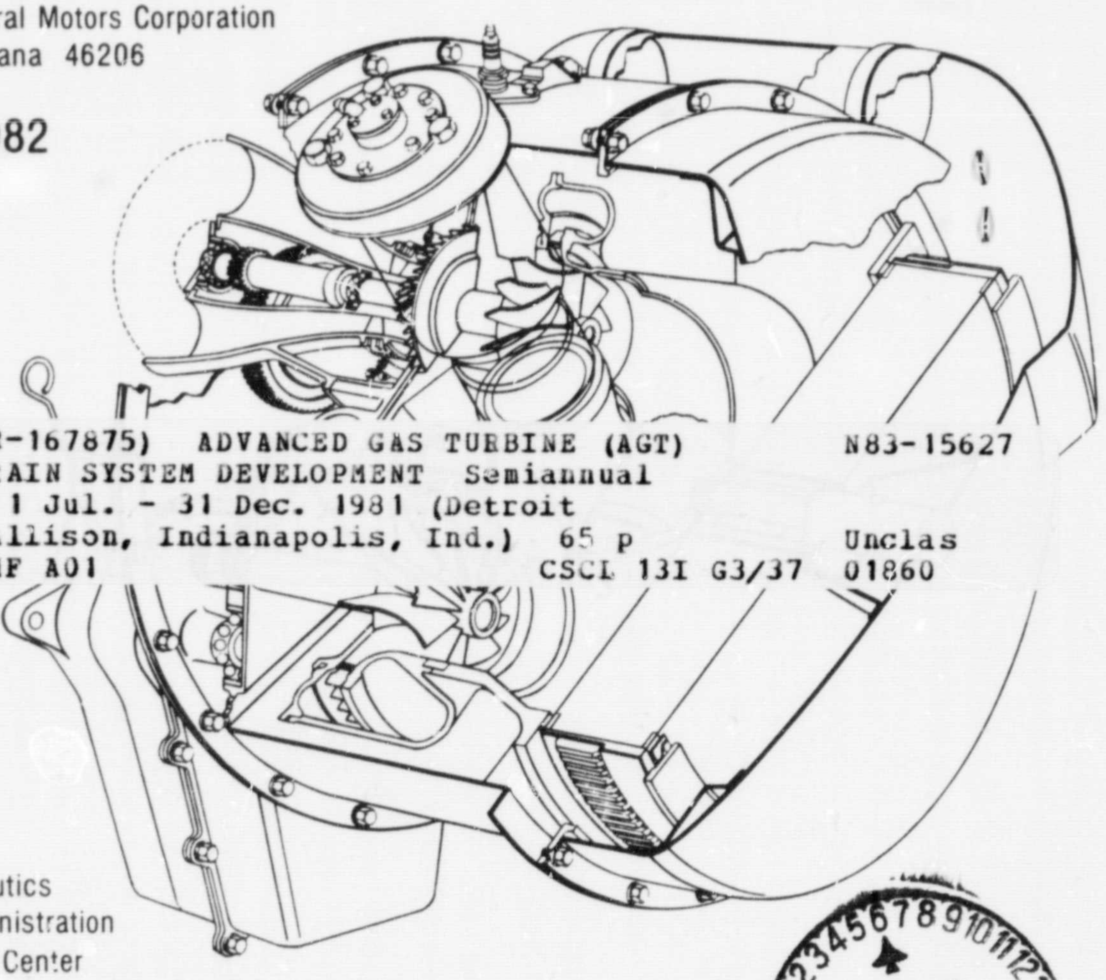

(NASA-CR-167875) ADVANCED GAS TURBINE (AGT) POWER-TRAIN SYSTEM DEVELOPMENT Semiannual Report, 1 Jul. - 31 Dec. 1981 (Detroit Diesel Allison, Indianapolis, Ind.) 65 p HC A04/MF A01 CSCL 13I G3/37 N83-15627 Unclas 01860

Prepared for
National Aeronautics
and Space Administration
Lewis Research Center
Cleveland, Ohio 44135
Contract DEN 3-168

For U. S. Department of Energy
Conservation and Renewable Energy
Office of Vehicle and Engine Research and Development

FOREWORD

This report presents a technical summary of the Detroit Diesel Allison (DDA) project to develop an automotive gas turbine power-train system under NASA Contract DEN3-168 (Department of Energy funding). It covers the 6-month period July 1981 through December 1981.

The basic objective of this project is to develop and demonstrate, by May 1985, an advanced automotive gas turbine power-train system that will, when installed in a 1985 Pontiac Phoenix vehicle of 1360 kg (3,000 lb) inertia weight, achieve a fuel economy of 18 km/L (42.5 mpg), meet or exceed the 1985 emission requirements, and have alternate fuel capability.

Several General Motors Divisions and other companies are major contributors to this effort. They are: Pontiac Motor Division—vehicle, Delco Electronics Division—electronic control, Delco Remy Division—starter/boost motor, Harrison Radiator Division and Corning Glass Works—regenerator, Hydramatic Division—transmission, the Carborundum Company and GTE—ceramics.

The DDA Program Manager for the AGT 100 is H.E. (Gene) Helms; design effort is directed by James Williams; materials effort is directed by Dr. Peter Heitman; and project effort is directed by Richard Johnson. The Pontiac effort is headed by James Kaufeld, and the Delco Electronics work is managed by Robert Kordes. The NASA AGT 100 Project Manager is Paul T. Kerwin.

PRECEDING PAGE BLANK NOT FILMED

TABLE OF CONTENTS

LIST OF ILLUSTRATIONS

LIST OF TABLES

Summary

Engine/Power-Train Development

An accelerated build schedule was started in August to have an engine operating by mid 1982. By the end of December 1981 all castings had been received and 62% of purchase parts were in-house. All parts are scheduled to arrive by the end of February. Performance computer programs were updated to include gasifier and power turbine test rig maps. Performance curves were generated, illustrating the evolution from the first engine build using many metal parts to the fully developed RPD engine using ceramics.

Compressor Development

Activities included testing two builds of the compressor incorporating the first aerodynamic modification of the original design. This modification included a reduction in blade thickness and a reduction in diffuser throat area. Testing of the impeller in BU5 was successful. Complete speed lines were obtained at 50%, 70%, 80%, 90%, 95%, and 100% speeds with zero inlet prewhirl. High speed flow, pressure ratio, and efficiency showed significant increases for BU5 over a previous BU3.

Gasifier Turbine Development

Aerodynamic design has been completed for the Mod I turbine. Blade books and master charts were generated for the rotor, vanes, vane slots, and endwall contours for both metal and ceramic configurations. Rig test results for the RFD configuration were reevaluated after the rig torquemeter was recalibrated. Good agreement was generally achieved between the torquemeter and temperature efficiencies at high expansion ratios. Hysteresis and load fluctuations of the test module caused some discrepancies at reduced expansion ratios. Efficiencies based on temperature appear to be the most characteristic. Prototype ceramic turbine wheel development continued with additional representative wheels being spun to failure in cold spin tests. The failure speed distribution appears to follow a two-parameter Weibull curve from which a Weibull modulus (strength) of 7 can be inferred.

Power Turbine Development

Aerodynamic design has been completed for the Mod I turbine. Blade books and master charts have been generated for the rotor, vanes, vane slots, and endwall contours for both the ceramic and metal configurations. The RPD engine turbine aerodynamic definition is identical to rig hardware with the exception of a correction for hot-to-cold thermal/mechanical contraction.

Analysis has been completed on the power turbine rig data. The power turbine operated close to RPD design expectations over a broad range. Higher efficiencies were obtained at the maximum power point as a result of the rotor operating more efficiently than predicted.

The DDA radial turbine performance computer code was modified to provide a close match with experimental flow rate, work, and efficiency.

Combustor Development

Four alternate combustor concepts were analytically evaluated: staged cyclone, two-stage with radial swirlers (two concepts), and two-stage with one radial and one axial swirler. The staged cyclone concept was not pursued because of risk. There was a good deal of similarity in performance among the other three concepts. The selection was made on the basis of packaging ease within the engine compartment. The entire combustor can be fabricated in ceramic. Combustor testing using a preheater showed that (1) a source of ignition was not required to initiate combustion at high burner inlet temperatures (900°C [1652°F] range); (2) since auto ignition could take place, lean blowout did not occur; and (3) auto ignition did not occur in the prechamber. The emission results were encouraging; compared with previous tests the CO level remained the same but the NO_X level dropped an order of magnitude.

Regenerator Development

Design work was completed on the regenerator cover and the ceramic exhaust duct/regenerator seal platform. These designs will be used in the test engine with only minor modifications. The one-piece ceramic exhaust duct/seal platform has been predicted to have acceptable stress levels. Cold flow tests at two conditions show that the velocity distribution is acceptably flat at 48 km/h (30 mph) conditions but has a local peak at 100% power.

Secondary Systems

Structural design work was completed on the combustion case assembly, insulation, ceramic and metal scrolls, and the test engine limit stack. Two combustion cases are being fabricated in AISI 410 steel. The layout describing the simplified gear train was completed along with detail drawings of component parts. Starter/burst motor brush durability tests have been conducted, and after 70,000 cycles the standard motor brushes are within acceptable wear limits. Brush lifting mechanism wear tests were also satisfactory.

Controls Development

A preliminary electrical control system for the first scheduled engine run has been designed. It will be a modified unit from another DDA program. All electronic boards have been built, and only thermocouple channels need to be added. The functions of a control console have been established, and a preliminary schematic has been designed for an engine test simulator. Coding of the control software has started.

Materials Development

Thermal barrier work was conducted by Carborundum Co. (CBO) using mullite, and DDA conducted parallel programs with zircon and zirconia. Barrier materials have been produced using both mullite and cordierite, and techniques have been developed whereby sol-gel powders are used for hot pressing and pressureless sintering. Pertinent ceramic processing variables have been determined for fabricating fine-grained, low-porosity zircon based materials. Partially stabilized zirconia materials were prepared for DDA evaluations by two different vendors. Both materials have an average strength greater than 206.8 MPa at 1000°C (30 ksi at 1832°F).

Silicon carbide structural parts have been fabricated and tested. These include the gasifier rotor, combustor assembly, and the gasifier scroll, duct, backplate, and vanes. Spin tests of the ceramic rotors have been conducted in July and October this period. Seventy-seven percent of the rotors of the last four lots have reached burst speeds in excess of 100% design speed.

Supportive Manufacturing, Cost, and Marketability

Manufacturing feasibility studies by Pontiac Motor Division (PMD) have led to several design changes to improve manufacturing feasibility and/or reduce cost. To date, PMD has received 65 designs, over half of which have been received or are in process of review. PMD is also conducting a cost analysis for the total engine. There are 286 parts or assemblies to be received, and drawings for 248 have been received by PMD.

Introduction

This is one of a series of semiannual reports documenting work performed on an Advanced Gas Turbine (AGT) power-train system development project for automotive applications. The work is performed under NASA/DOE contract DEN3-168. The objective of the project is to develop an experimental power-train system that demonstrates (1) a combined cycle fuel economy of 17.9 km/L (42.5 mpg) using diesel fuel No. 2 in a 1984 Pontiac Phoenix of 1364 kg (3000 lbm) weight on a 15°C (59°F) day; (2) emission levels less than federal standards; and (3) the ability to use a variety of fuels. It is intended that the technology demonstrated through this project would assist the automotive industry in making a go/no-go decision regarding the production engineering development of gas turbine power-trains.

In meeting the project objective, the design is constrained to (1) achieve reliability and life comparable to conventional 1985 vehicles; (2) achieve initial and life-cycle power-train costs competitive with 1985 power trains; (3) demonstrate vehicle acceleration suitable for safety and maneuverability; and (4) meet 1985 federal vehicle noise and safety standards.

A team concept is used in this project, with many of the team members being General Motors Divisions. DDA is the prime contractor and team leader with responsibility for the overall power train and controls. Pontiac Motor Division (PMD) has vehicle responsibility. Delco Electronics will develop the electronic control, and Delco Remy will develop the starter/boost system for the engine. Hydra-matic Division will produce the four-speed automatic transmission that will be used with the engine, and Harrison Radiator Division is involved in the regenerator design and fabrication. The primary non-GM groups on the team are Carborundum Co. (CBO), Corning Glass Works (CGW), and GTE Laboratories Inc., who are involved in the ceramic effort.

The current project began in October 1979. Establishing and maintaining a reference power-train design (RPD) is a continuing activity as is component development.

The RPD is a preliminary engineering design of the power-train system that has the best potential for meeting the goals and objectives of the project. It can incorporate timely emerging technologies and will be updated as project activity progresses.

In this current program the RPD evolved from earlier studies and is presented as a "concept" of a fully developed production power-train. The overall program plan is currently being reviewed and replanned to accommodate changes at DOE resulting from new direction by the Administration.

The main development challenges in the program are in building small, high-performance gas turbine components and developing ceramic components for the required high engine cycle temperatures that are price competitive and can be produced in an automotive production environment. Because of the small-size engine (0.35 kg/s [0.76 lbm/sec] airflow), extensive rig testing is being performed in component development. A major ceramic component development program is being pursued, and the ultimate success of the engine depends on the success of this activity.

This report is structured on a component basis (e.g., all work relating to the gasifier turbine rotor, including rig work and ceramic rotor development, is discussed as a part of the gasifier turbine section). Exceptions to this are functional areas that are not peculiar to any one major component: engine subsystems, cover structures, gearbox and power transfer, rotor bearings, shafts/seals, and secondary flow. There are separate sections for materials development and controls development.

Certain sections are omitted in this report because no effort was expended in those areas. These sections—Vehicle System Development, Reference Power-Train Design, and Transmission Development—are identified in the Table of Contents to preserve continuity.

II. Engine/Power-Train Development

2.2 Mod I

Engine Fabrication

The parts acquisition schedule for the accelerated build program initiated in August is shown in Figure 1. Drafting for the Mod I engine was completed on 1 October. At this time purchase orders had been placed for approximately 50% of the parts required for two engines plus spares. All purchase orders were placed by 7 November, including 65 control and test items added after the schedule was established. Purchase orders account for 96% of the total requirement. Bimonthly contacts are being made with each supplier.

All castings have been received, and 62% of the purchase parts were in-house at the end of the year. This activity was slightly behind schedule because shipments were held at suppliers' facilities over the year-end holidays. Parts in transit at the beginning of 1982 will overcome this slight schedule deficiency. All significant parts are scheduled to be delivered by the end of February.

Ceramic Components

Figure 2 shows static ceramic components received from several companies instrumental in developing a variety of development processes. The zirconia components were supplied by the Kyocera/Feldmuhle consortium. These sintered isopressed parts are incorporated as thermal barriers between the turbines and static structure in the engine design.

The remaining parts shown in Figure 2 are silicon carbide. With the exception of the two couplings and piston ring, supplied by Pure Carbon, the silicon carbide parts are components of the prototype combustor assembly.

All of the Kyocera SiC parts are isopressed.

All CBO parts are sintered SiC and are isopressed and green machined with the exception of the combustor body, which is slip cast.

The Pure Carbon parts are isopressed siliconized SiC with the exception of the pilot flame holder, which is extruded. The couplings and piston ring allow relative movement between gasifier and power turbine ducting.

The two combustor bodies supplied by Corning/Annawerk represent different sintering and reaction bonding processes.

These parts represent a significant cross section of technology development that has been evaluated for the AGT 100 engine.

Performance

Performance computer programs were updated to include gasifier and power turbine test rig maps. These programs include calculating turbine test rig (equivalent) expansion ratio at rig conditions for a table look-up of turbine flow and efficiency, as well as calculating an efficiency decrement as a function of turbine axial and radial clearance.

Component test rig performance maps were used as a basis to predict the various engine performance curves (current components) and are presented in Figure 3. These maps included compressor rig Build 2 (BU2) adjusted for estimated heat transfer effects, gasifier turbine rig BU58, and power turbine rig BU59. In Figure 3 each line of specific fuel consumption versus power represents a different state of development of the AGT 100. Collectively they illustrate the evolution of performance from BU1 to the fully developed RPD.

The uppermost line (BU1) is based upon 1080°C (1976°F) turbine temperature (metal rotors), current components, higher-than-design engine leakage, and wide operating clearances. Maximum power is estimated to be 26.8 kW (36 hp) based upon a 29°C (85°F) day with best fuel consumption of 340.6 mg/W·h (0.56 lb/hp-hr). Through development, the engine leakage and operating clearances will meet the design goals represented by the second line of 35.0 kW (47 hp) maximum power and 292.0 mg/W·h (0.48 lb/hp-hr) best fuel consumption. The third line, showing 60.4 kW (81 hp) maximum power and 231.1 mg/W·h (0.38 lb/hp-hr) best fuel consumption, can be achieved by adding the full complement of ceramic components, which allows operation at 1288°C (2350°F); the current level of components was assumed for illustrative purposes. The RPD line, showing 64.1 kW (86 hp) maximum power and 194.6 mg/W·h (0.32 lb/hp-hr) minimum fuel consumption, is reached when both ceramic and fully developed components are incorporated into the engine.

PRECEDING PAGE BLANK NOT FILMED

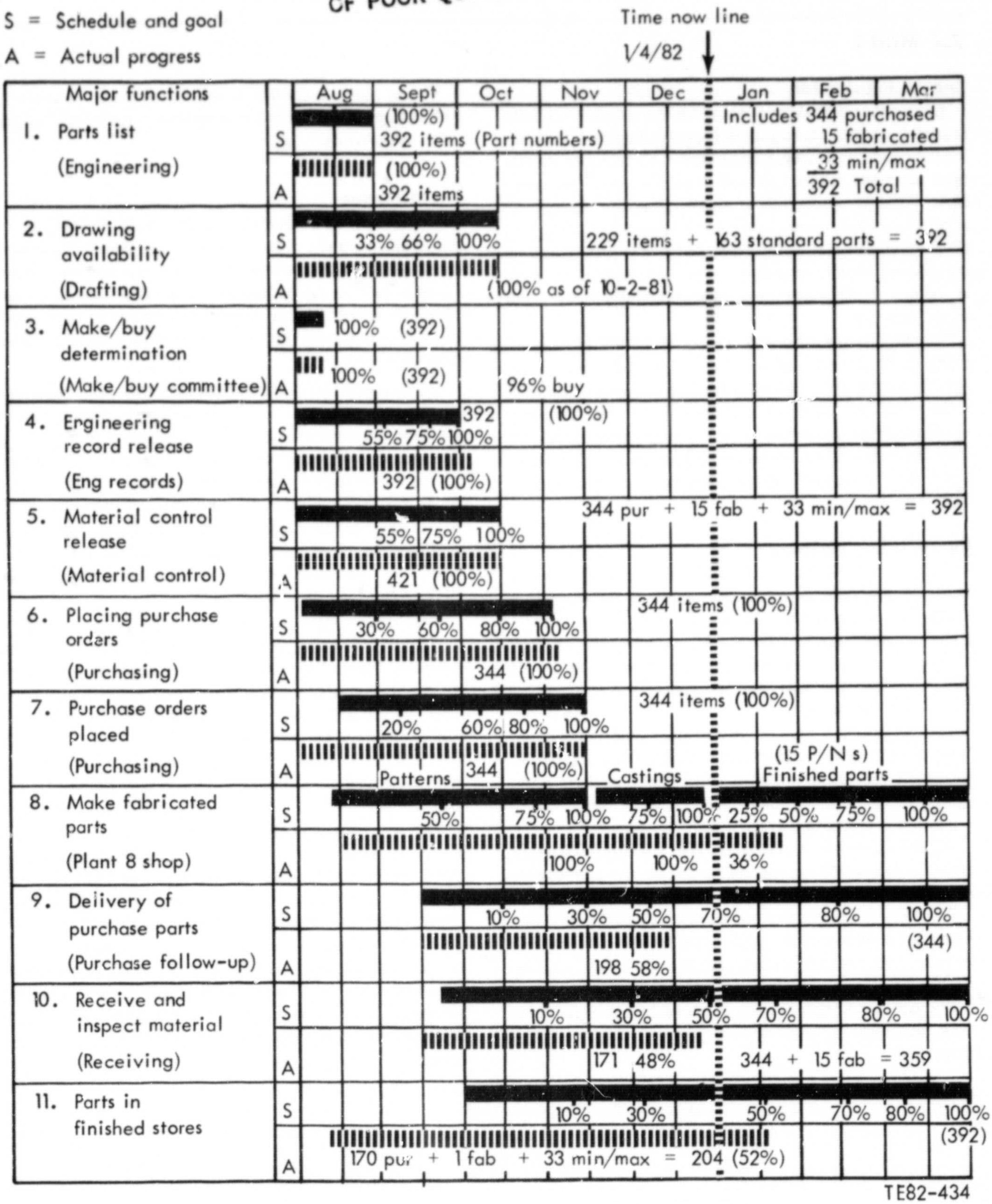

Figure 1. Parts acquisition schedule for the accelerated build program.

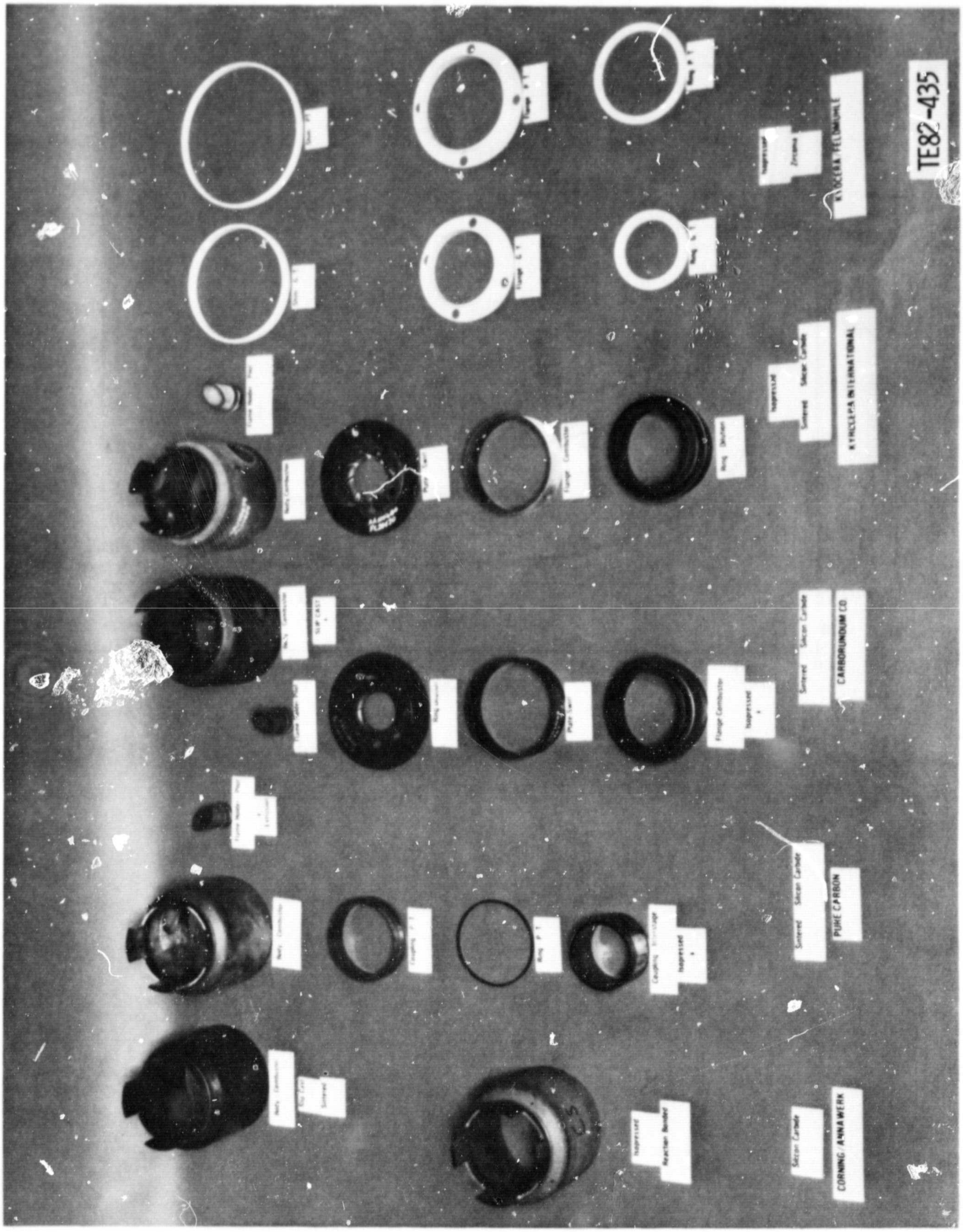

Figure 2. Static ceramic components.

ORIGINAL PAGE
BLACK AND WHITE PHOTOGRAPH

ORIGINAL PAGE IS
OF POOR QUALITY

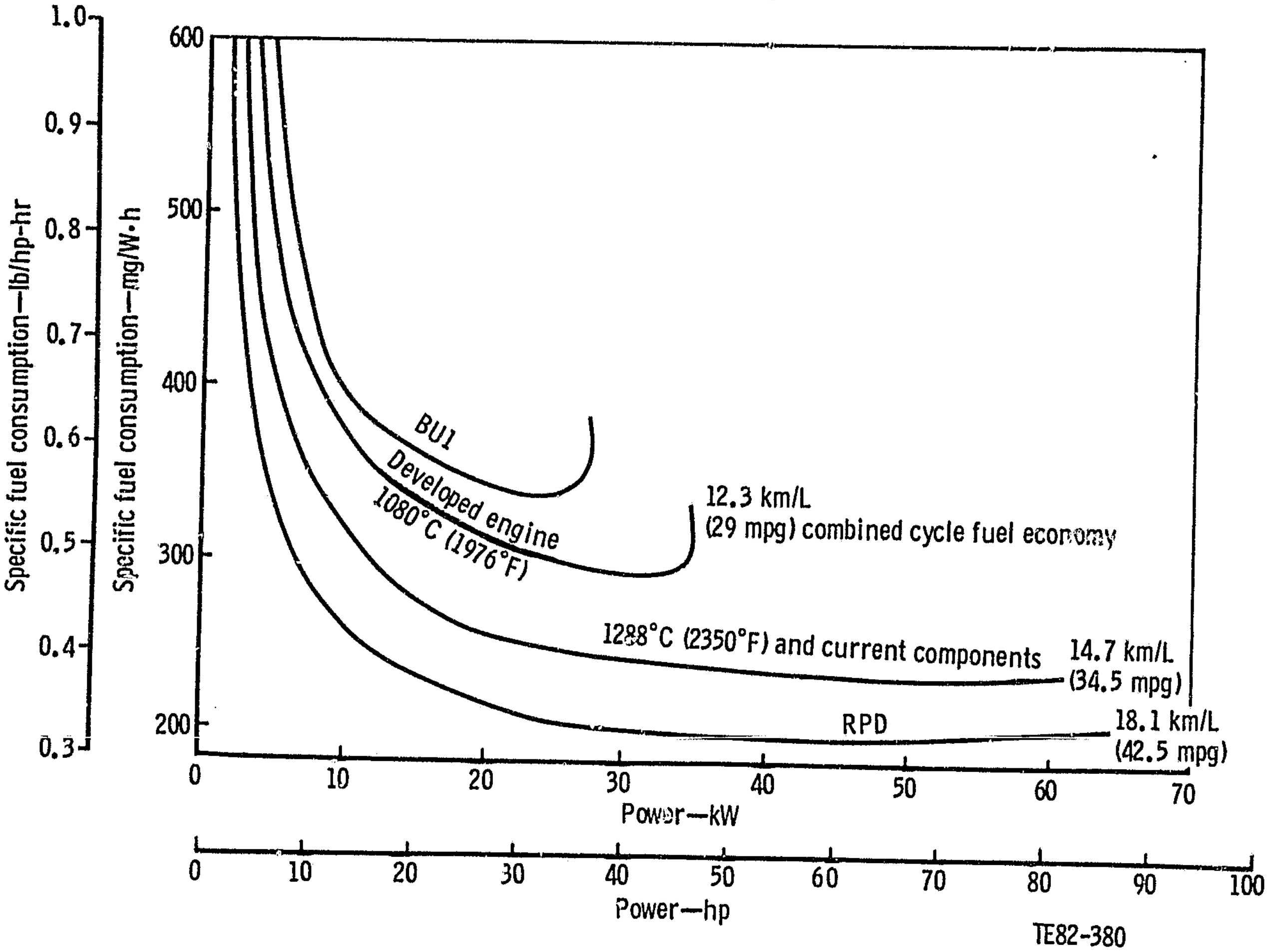

Figure 3. Performance evolution (29°C, 85°F day).

III. Compressor Development

3.1 Compressor Aerodynamic Development

Compressor development activities were primarily limited to testing two builds of the AGT 100 compressor, CX40 BU4 and BU5. These tests incorporated the first aerodynamic modification of the original design. The modification included a reduction in impeller blade thickness and a reduction in diffuser throat area. Build 4 testing was prematurely terminated due to a failure of piston ring seals in the rear compressor bearing compartment. No flow path hardware distress was observed, and subsequent testing was successfully completed as BU5 during September.

Rig Test Program—CX40 BU4 and BU5

The best calibration of the "as designed" configuration is given by the BU3 test results shown in Figure 4. This build incorporated the engine type axial inlet and the alternate inlet guide vanes (IGVs). As shown in Figure 4, design point flow and pressure ratio were demonstrated with sufficient surge margin to accommodate all expected engine operational requirements. Operating line efficiency levels were optimized at part speed, at which a majority of engine operation is expected to occur. High-speed efficiency (above 90% speed) dropped below part-speed levels.

A detailed analysis of BU3 data indicated that the high-speed efficiency drop-off was due to an apparent inducer choking condition. This fact is most clearly indicated by the measured inducer shroud static pressure distribution. Converted to an equivalent static pressure recovery coefficient, $C_{p_{imp}}$ (indicative of relative velocity diffusion), the measured static pressures at design speed and flow, showed significant acceleration into the inducer throat region (see Figure 5). This initial acceleration resulted in reduced overall impeller pressure recovery and, consequently, reduced stage pressure ratio and efficiency.

To reduce inducer choking effects, the inducer throat area was increased by uniformly removing approximately 0.25 mm (0.010 in.) from the suction surface of all main blades and splitters. As a part of reducing blade thicknesses, the blade surfaces were polished to improve surface finish from 1.27-1.78 microns (50-70 microinches) to 0.51-0.76 microns (20-30 microinches). In anticipation of increased impeller pressure rise capability, the diffuser throat area was reduced by 10% to maintain match point flow near design levels.

This configuration went to the test stand as CX40 BU4 early in August. Data were obtained at 50%, 70%, and 80% speeds. Pressure measurements in the rear compressor bearing compartment and a sudden increase in rig vibration levels indicated a failure of the piston ring

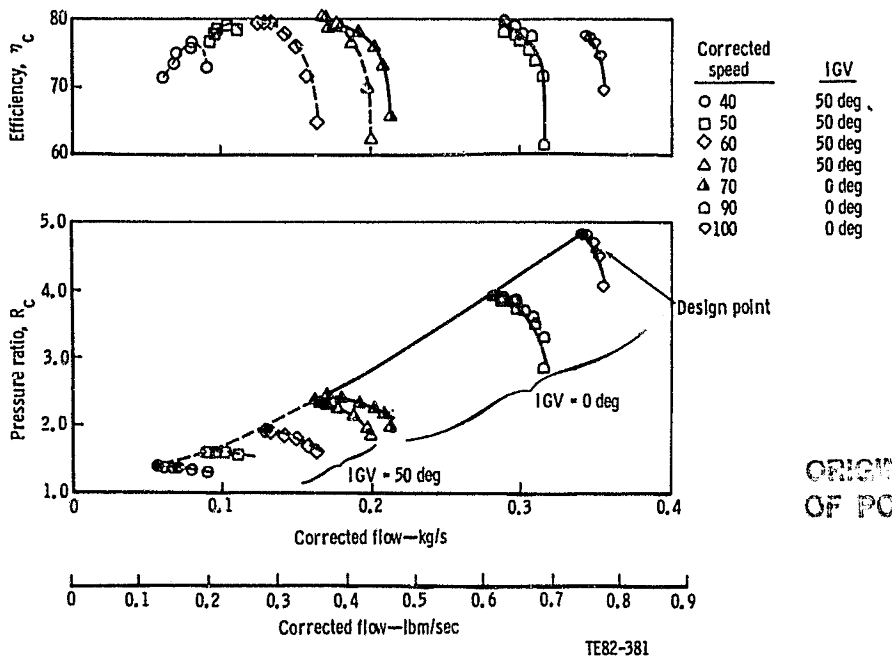

ORIGINAL PAGE IS OF POOR QUALITY

Figure 4. Compressor performance, BU3.

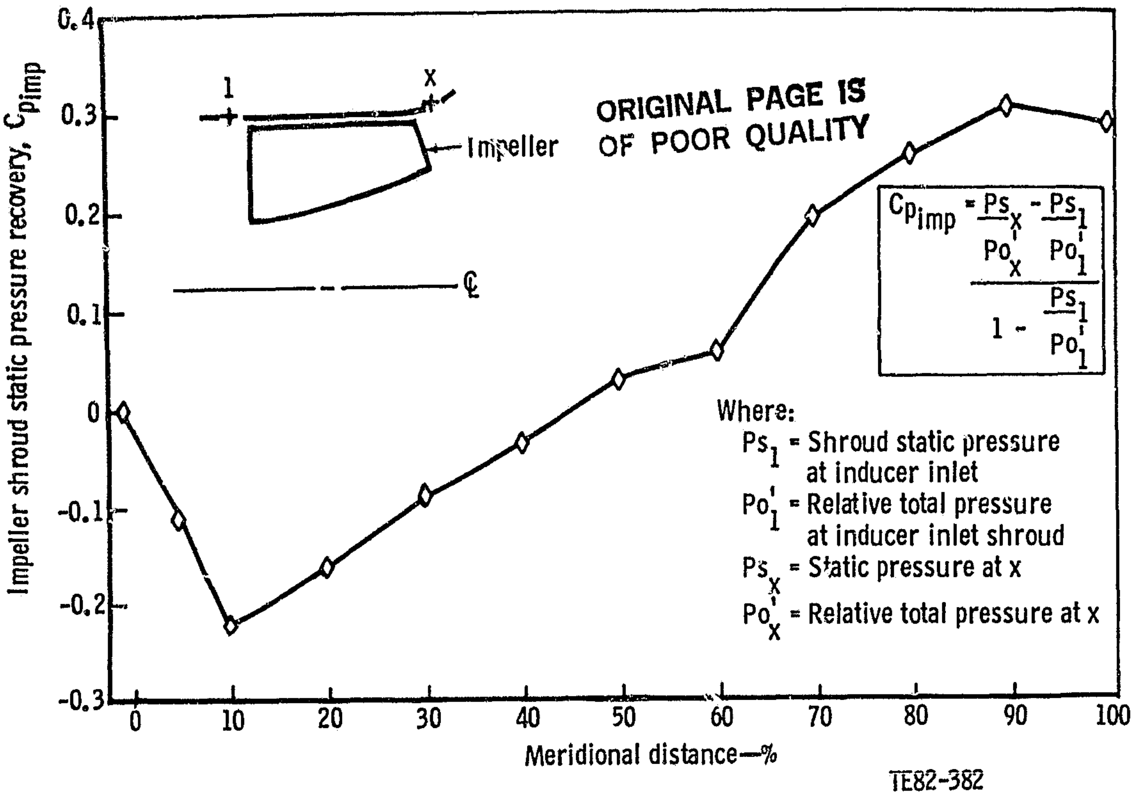

Figure 5. Impeller shroud inlet to exit static pressure recovery, CX40, BU3 at design speed and flow.

seals in this area. The rig was removed from the test stand, and the piston ring failures were confirmed. Visual inspection of the seals indicated that the most likely reason for the seal failure was seal rotation within the stationary housing. In an attempt to prevent seal rotation, the rig was modified to incorporate axial springs to preload the ring seals against the housing. The rig was then reassembled as BU5, and the first data were obtained on 17 September 1981. Performance mapping of BU5 was completed during September. Complete speed lines were obtained at 50%, 70%, 80%, 90%, 95%, and 100% speeds with zero inlet prewhirl. These data are shown in Figure 6. In addition, the following speed lines and IGV settings were obtained:

Corrected speed—%	IGV angle (deg)
50	25, 50
70	25, 50
80	15, 25
90	15

These data are presented in Figure 7

Overall performance data from BU5 are compared with data from BU3 in Figure 8 for high-speed and Figure 9 for low-speed operation. In general, high-speed flow, pressure ratio, and efficiency showed significant increases for BU5 relative to BU3, as shown in Table I.

Part-speed efficiency was lower for BU5 than for BU3. Efficiency differences varied from −1% at 50% speed to −2% at 70% speed. The BU5 surge margin was greater at all points than was the BU3 surge margin, with maximum differences occurring at 100% speed.

Detail measurements of the BU5 impeller blading are proceeding and will be followed by additional internal analysis to fully understand the observed BU3-BU5 performance differences. Because the part-speed performance was improved and the Rc was nearer to design, the BU3 configuration was selected for initial engine testing.

3.2 Compressor Mechanical Design

Compressor rig testing has provided insight for selected design modifications that would benefit engine performance or life.

The main shaft seals were subject to metal pickup, forcing them to rotate with the shaft and eventually leading to failure. To prevent this from happening on engine hardware, the running clearance was increased and spring washers were added to stop rotation. Design changes to engine hardware were also made so that engine components would reflect the designs used on the test rig (BU3). This configuration will be incorporated in the initial build of the Mod I engine.

ORIGINAL PAGE IS
OF POOR QUALITY

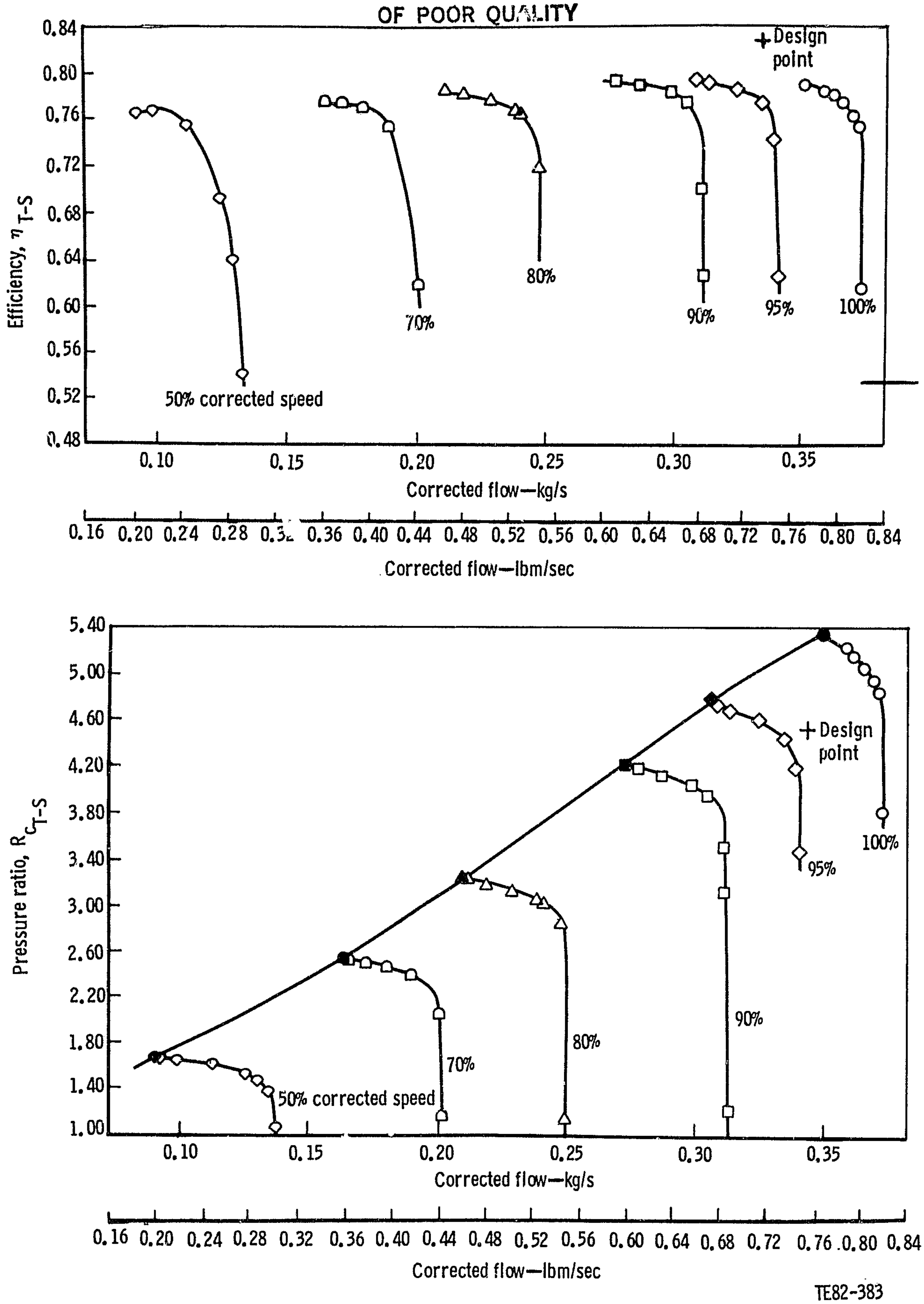

Figure 6. Compressor performance, BU5.

ORIGINAL PAGE IS
OF POOR QUALITY

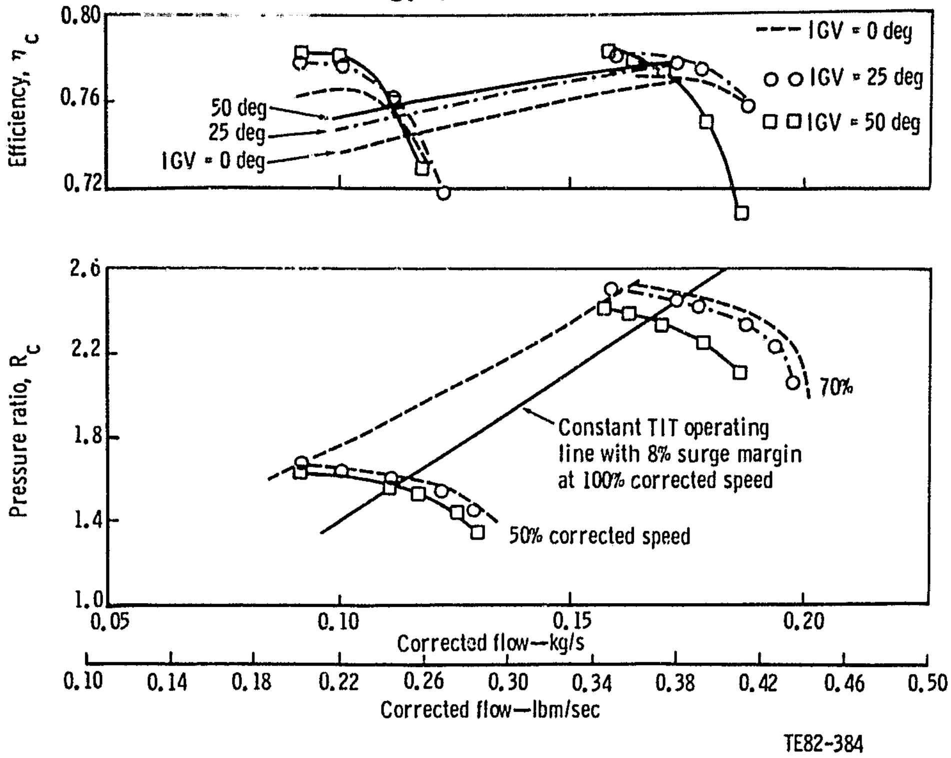

Figure 7. Effect of variable IGV on compressor performance, CX40, BU5.

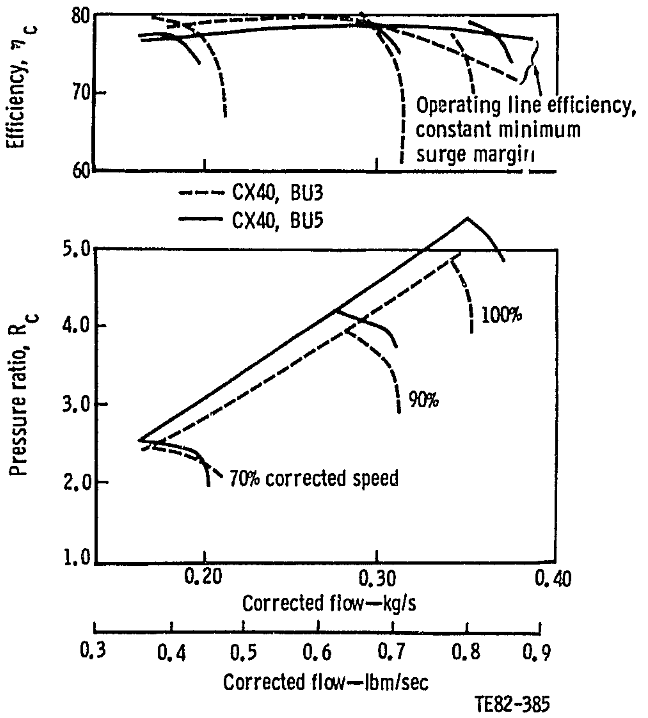

Figure 8. High-speed performance comparison, IGV = 0 deg.

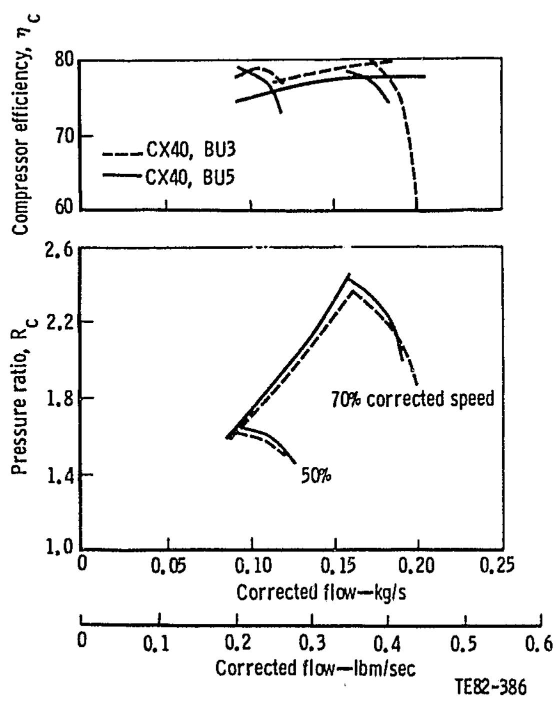

Figure 9. Low-speed performance comparison, IGV = 50 deg.

ORIGINAL PAGE IS
OF POOR QUALITY

Table I. Performance comparison at 100% speed.*

	Design	BU3	BU5	Change—%
Corrected flow—kg/s (lbm/sec)	0.347	0.346 (0.765)	0.362 (0.800)	+ 4.6
R_C	4.5	4.6	5.13	+11.6
η_c	0.828	0.755	0.780	+ 2.5
Choke flow—kg/s (lbm/sec)	—	0.352 (0.777)	0.372 (0.822)	+ 5.8

*Data were taken at a point with 8% surge margin at 100% speed.

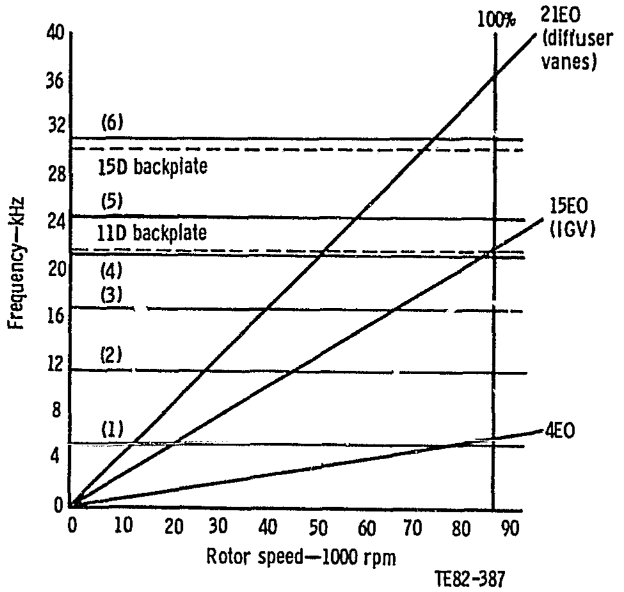

Figure 10. Full blade frequency diagram, 1.27 mm (0.050 in.) backplate thickness.

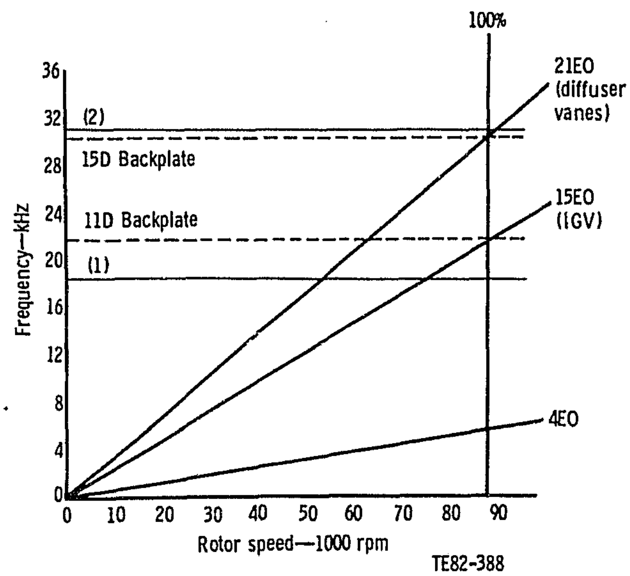

Figure 11. Splitter blade frequency diagram, 1.27 mm (0.050 in.) backplate thickness.

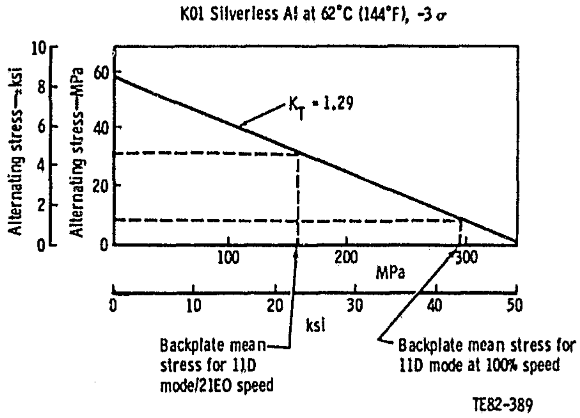

Figure 12. Goodman diagram compressor backplate.

On completion of the first phase of rig testing, the impeller was found to be cracked in two places. The larger crack originated on the suction side of the splitter blade adjacent to the fillet, at exit, traversing radially inward about 4.76 mm (3/16 in.), and the smaller was about 1.59 mm (1/16 in.) at 180 deg from the larger. Blade frequency diagrams represented in Figures 10 and 11, show potential excitations in the operating speed range and backplate resonance with the diffuser vanes near the 70% speed point and also 100% speed.

The maximum vibratory stress occurs at the failure location, and the allowable stress for the 1.3 mm (0.050 in.) thick backplate is ±33.1 MPa (4.8 ksi). The backplate mean stress for 11D mode and 21st engine order speed is 29.6 MPa and 11.0 MPa (4.3 ksi and 1.6 ksi) for 11D mode at 100% speed, as shown in Figure 12. The backplate surface between the blades and on the backplate tip for approximately 12.7 mm (0.5 in.) will be shot peened, and the backplate thickness will be increased from 1.3 mm to 2.6 mm (0.050 in. to 0.080 in.) to extend the fatigue endurance of the impeller.

To keep the idle temperature high for good fuel economy, the IGV mechanism was modified to reflect a greater range of vane movement to throttle the airflow to the compressor. A curve of vane travel versus actuator stroke was prepared (see Figure 13) to provide information for the analysis of the engine control unit.

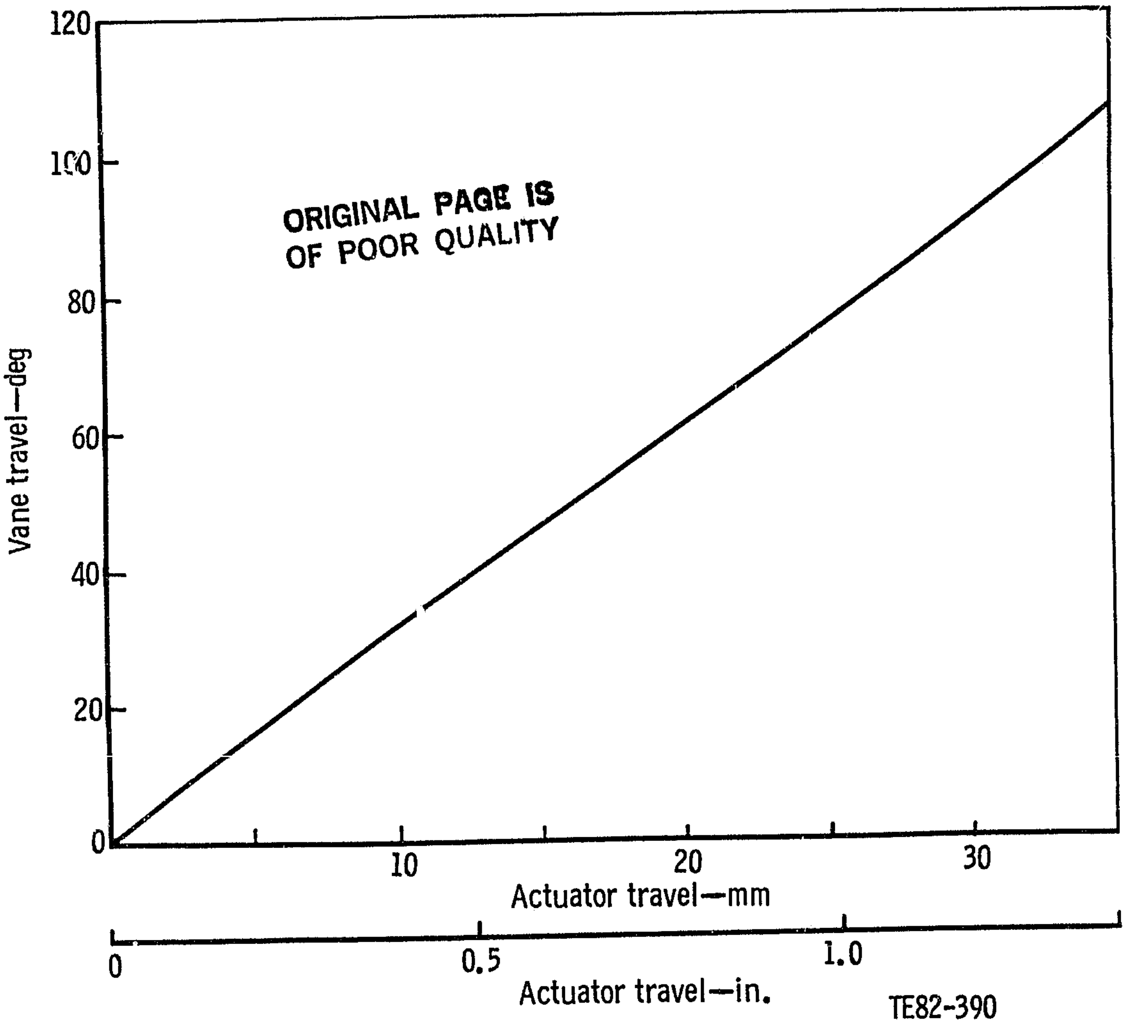

Figure 13. IGV travel versus actuator stroke.

IV. Gasifier Turbine Development

4.1 Gasifier Turbine/ Aerodynamic Development

High efficiency over a broad operating range is the primary goal for the gasifier turbine. The aerodynamic design to achieve this goal must be consistent with stress, heat transfer, vibration, and mechanical design requirements. To be competitive in the automotive market, this goal must be achieved with recognition of the requirement for low cost and low inertia.

During this period aerodynamic design has been completed for the Mod I turbine. Blade books and master charts have been generated for the rotor, vanes, vane slots, and endwall contours for both the ceramic and metal configurations. The RPD engine turbine aerodynamic definition is identical to rig hardware, with the exception of a correction for hot-to-cold thermal/mechanical contraction.

The gasifier turbine rig test results were reevaluated based on recalibration of the rig torquemeter. Good agreement was generally achieved between torquemeter and temperature efficiencies at the higher expansion ratios. At the reduced expansion ratios, the torquemeter efficiencies exceeded the temperature efficiencies by a substantial amount. The scatter and high efficiencies associated with low torquemeter readings are attributed to hysteresis and load fluctuations of the turbine test module. The variation in module loss contributes significantly to efficiency determination due to the low output torque of the turbine. Efficiencies based on temperatures appear to be most characteristic of turbine performance.

Analysis has been completed on the gasifier turbine rig data. Velocity diagrams and element losses generated for each test data point revealed that vane losses were larger than predicted for the RPD design. Through development of the vane row, an efficiency improvement of up to two percentage points appears possible for the gasifier turbine.

The DDA radial turbine performance computer code was modified to provide a close match with experimental flow rate, work, and efficiency. This modified program was then used to specify the vane width and estimate performance for the first engine build.

4.2 Gasifier Turbine Mechanical Development—Mod I, Metal Scroll

The gasifier turbine scroll description and a view of the cross section are shown in Figure 14.

ORIGINAL PAGE IS OF POOR QUALITY

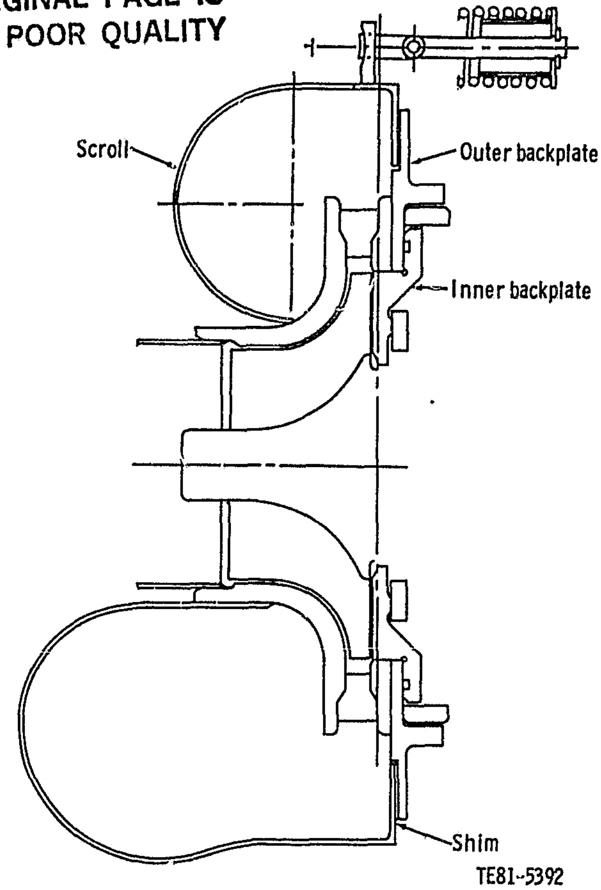

Figure 14. Metal gasifier turbine scroll.

The Mod I engine has a metal gasifier turbine rotor instead of a ceramic one, and the shaft dynamic analysis showed that the bend mode frequency was too close to the operating speed range. Several design changes were made to increase the bend mode frequency, and the No. 2 bearing isolator spring rate was increased from 3500 kN/m to 7000 kN/m (20,000 lb/in. to 40,000 lb/in.). The higher spring rate was achieved by modifying the isolator sleeve to accommodate two 3500 kN/m (20,000 lb/in.) springs.

The aerodynamic design review of the vanes based on rig test results was completed, and the vane shape and setting angle selected is the same as tested in the rig. Two metal scrolls are being fabricated. One will be finish-machined for the first engine build, and the second will be completed except for the machining of the shroud and endwall contours. This will allow modifications to be made, if necessary, based on first engine test results.

4.3 Ceramic Rotor Design and Development

Process development on a prototype ceramic radial turbine wheel has continued at CBO during this reporting period. The prototype wheel is fully bladed and is very similar to the final RPD gasifier turbine design except for direction of rotation (blade camber) and a minor axial trimback of the exducer portion of the blade. Previous material and processing experimentation at CBO has led to a concentration of effort on injection molding this configuration using CBO's SASiC material. (See also subsection 9.2).

A number of wheels produced during this process development phase have been sent to DDA for evaluation. Rotors produced early were obviously flawed and were used primarily to develop a spin test procedure. Later wheels show fewer and less severe defects. Although few are flaw-free, as determined by conventional NDE techniques (visual, fluorescent penetrant, and X-ray), considerable improvement has been shown. Representative wheels have been spun to failure in a spin pit, and a summary of failure speeds is shown in Table II.

Evaluating the later lots statistically by ranking measured burst speed yields a distribution characteristic as shown in Figure 15. Figure 15 represents the study of a like family of rotors to ascertain the distribution of strengths. In this analysis an attempt was made to use rotors that had been processed in a quite similar manner. Lots 1, 2, and 3 were not used because they were fabricated very early in the development phase and were experiencing large changes in processing variables. Lot 6 was excluded from the analysis because those rotors also had substantial processing changes from lots 4, 5, and 7, and were judged to be unrepresentative of the other rotors. The failure speed distribution appears to follow a two-parameter Weibull curve, from which a material strength Weibull modulus of 7 can be inferred. Although the wheels have been processed with minor variations in composition, presintering treatment, sintering atmosphere, etc., the variation in strength indicates that the wheel material quality is approaching that achieved by injection molded MOR test bars. Further process optimization is being carried on by CBO.

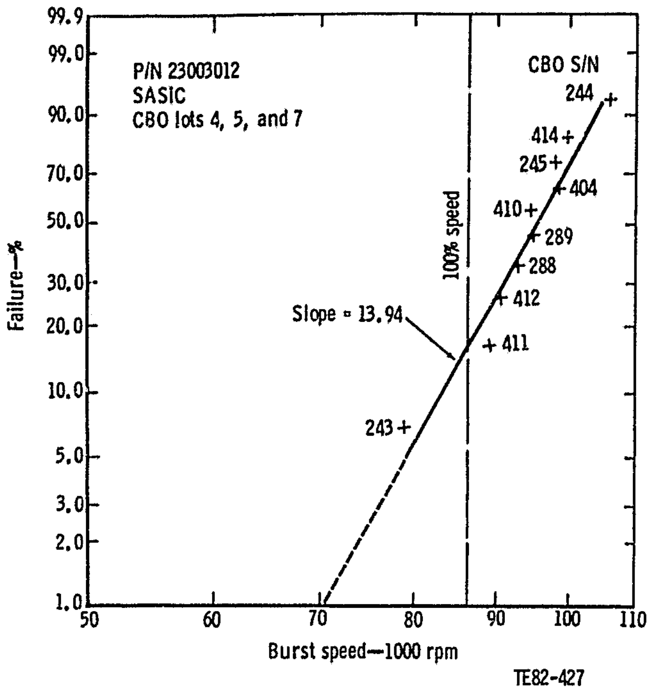

Figure 15. Weibull plot of rotor burst speed.

Table II. Cold spin burst test results.

CBO S/N	Burst speed (% of design*)	Date received	Lot No.
112	39	11-80	1
112	14	11-80	
115	36	11-80	
145	30	11-80	
001	54	2-81	2
004	63	2-81	
011	69	2-81	
236	17	3-81	3
238	102	3-81	
240	71	3-81	
242	83	3-81	
243	92	5-81	4
244	123	5-81	
245	115	5-81	
288	108	6-81	5
289	111	6-81	
296	76	7-81	6
297	95	7-81	
303	116	7-81	
410	111	9-81	7
404	114	9-81	
411	104	9-81	
412	106	9-81	
414	116	9-81	

*100% design speed = 86,240 rpm

A cold spin burst test characteristic has also been estimated, assuming that material strength levels meet design goals. Finite element analyses of a worst case cold start transient to part power have yielded the material strength requirement tabulated below:

Weibull modulus	Required median MOR strength MPa	ksi
8	540.5	78.4
10	430.2	62.4
12	383.4	55.6
14	350.9	50.9
18	313.7	45.5

Utilizing these strength values, a burst speed failure characteristic can be computed, assuming that the wheel is subjected to a cold spin test. Figure 16 indicates the

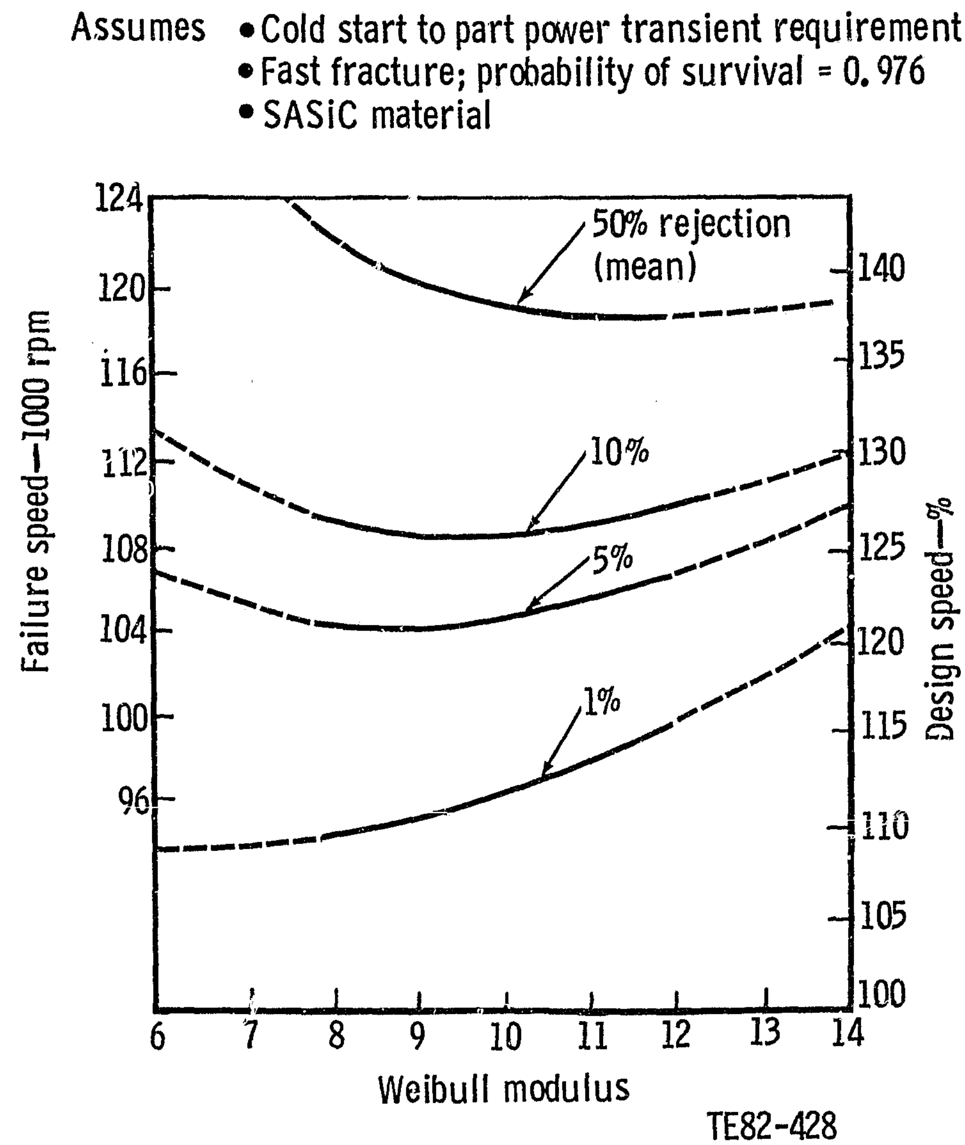

Figure 16. Cold spin burst test requirement for gasifier turbine wheel.

failure speeds at which various loss rates would occur. The mean failure speed is approximately 138% of maximum design speed. Assuming that a 10% rejection rate is a maximum acceptable level, a 110,000 rpm (127%) screening test level is indicated.

The difference in stress states between a cold spin and an engine transient is significant, and as a result, a cold spin test cannot be usefully employed as a true proof test. Proofing the wheels by cold spin testing to achieve the same transient local peak stress level would overproof large portions of the wheel and would cause excessive loss rates. This is due to the statistical nature of testing on ceramic materials and the stress/volume interaction. A cold spin test is, however, a useful tool in ascertaining overall material strength in the wheel itself and will be used accordingly.

ORIGINAL PAGE IS
OF POOR QUALITY

V. Power Turbine Development

5.1 Power Turbine Aerodynamic Development

The primary goal of the power turbine development is high efficiency over a broad operating range. The aerodynamic design to achieve this objective must be consistent with stress, heat transfer, vibration, and mechanical design requirements. To be competitive in the automotive market, the goal must be achieved with recognition of the requirement for low cost and low inertia.

Aerodynamic design has been completed for the Mod I turbine. Blade books and master charts have been generated for the rotor, vanes, vane slots, and endwall contours for both the ceramic and metal configurations. The RPD engine turbine aerodynamic definition is identical to rig hardware with the exception of a correction for hot-to-cold thermal/mechanical contraction.

Analysis of the power turbine rig data has been completed. The power turbine operated close to RPD design expectations over a broad range. Higher efficiencies were obtained at the maximum power point as a result of the rotor operating more efficiently than predicted.

The DDA radial turbine performance computer code was modified to provide a close match with experimental flow rate, work, and efficiency. This modified program was then used to specify the vane width and estimate performance for the first engine build.

Interturbine Duct/Power Turbine Scroll Bench Rig

Fabrication, assembly, and instrumentation were completed for the experimental evaluation of the updated duct/scroll configuration. A schematic of the bench rig is illustrated in Figure 17. Instrumentation included power turbine vane inlet and exit total and static pressure, vane inlet swirl angle, and scroll and duct wall static pressures.

Testing has been conducted at the simulated maximum power operating condition. Preliminary assessment of the integrated mass averaged measured losses for the duct/scroll is summarized in Table III. Comparison of measured losses for the present scroll configuration and the previous configuration (tested October 1980) is shown in Figure 18. Circumferential variation in mass flow is less than ±5%. Further data analysis will be performed to provide a more accurate loss assessment and to identify vane incidence angle variation with circumferential position.

Table III. Measured interturbine duct and power turbine scroll total pressure loss.

Duct inlet swirl angle	Duct/scroll total pressure loss ($\Delta P_T/P_T$) Present configuration	Previous configuration
20° CCW	2.30%	—
10° CCW	1.51%	1.27%
0°	1.71%	1.32%
10° CCW	1.90%	1.35%
20° CCW	2.92%	1.48%

CW = clockwise looking downstream

CCW = counterclockwise looking downstream

5.2 Power Turbine Mechanical Development—Mod I Metal Scroll

The power turbine scroll cross section is shown in Figure 19. The design aspects of this scroll are similar to those reported for the gasifier turbine scroll in Section 4.2.

The vane aerodynamic design and setting angle was fixed as that tested in the rig. Scroll fabrication has begun on one scroll, which will be finish machined. A second scroll will be partly machined with stock left in selected areas to allow possible modifications as testing progresses.

PRECEDING PAGE BLANK NOT FILMED

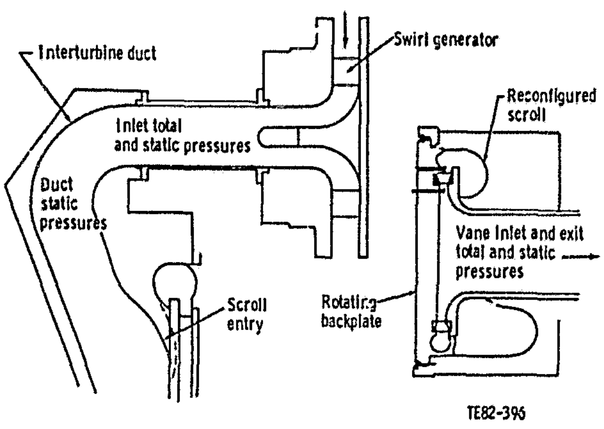

Figure 17. Interturbine duct and power turbine scroll bench rig.

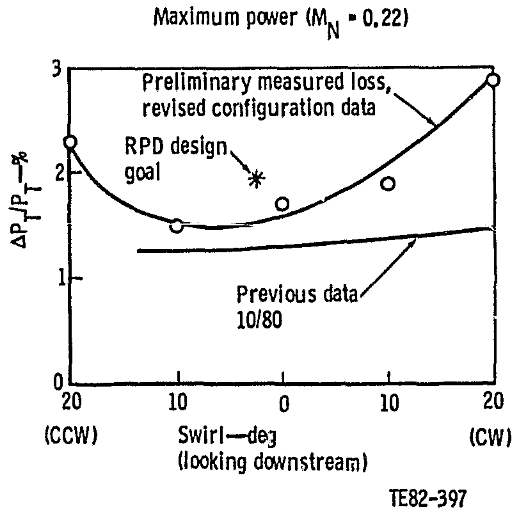

Figure 18. Interturbine duct and power turbine scroll loss comparison.

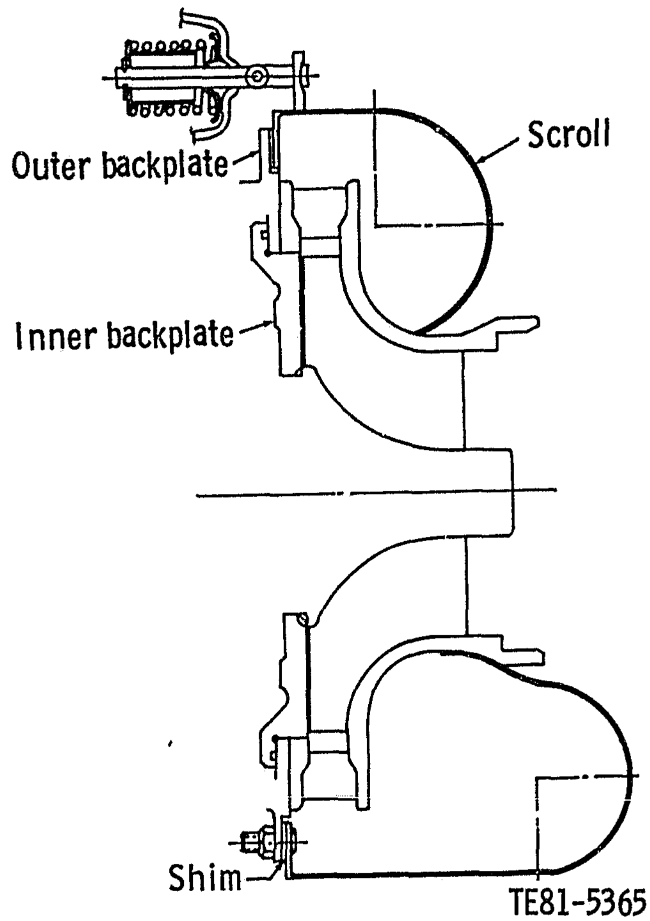

Figure 19. Metal power turbine scroll.

ORIGINAL PAGE IS OF POOR QUALITY

VI. Combustor Development

6.1 Combustor Development

Alternate Combustor

Four alternate combustor concepts (described in the previous semiannual report [Ref. 1]) were evaluated analytically using the COSMIC computer program (computation of swirl mixing in combustors): staged cyclone, two-stage with radial swirlers (two concepts), and two-stage with one radial and one axial swirler. As described in Ref. 1 the staged cyclone design was not pursued because DDA had limited experience with this type of combustor and development risk was higher than with the other alternate designs. The computer-generated flow fields were similar for the three alternate concepts considered the most viable. Because of the similarity the selection was made on the basis of packaging ease within the engine compartment. The design of this alternate combustor allows the entire structure to be fabricated in ceramic. Portions of a prototype combustor were fabricated in Hastelloy, however, to permit an early evaluation of this concept in a rig test. This design concept is shown in Figure 20 with flow streamlines for 96 km/h (60 mph) vehicle speed and 67% engine speed.

High-Temperature Air Preheater

In the first test of this preheater with the AGT 100 combustor, the maximum achievable burner inlet temperature (BIT) was 960°C (1779°F), 56°C (100°F) below the required level. Modifications were made whereby the blower that supplied combustion air to the preheater was removed and a connection made directly to the shop air supply. With this arrangement, the airflow to the preheater combustor was increased, and a BIT of 1080°C (1890°F) was achieved.

Based upon these successful tests with a shop air supply, it was concluded that a larger air blower was required and that some minor rework of the preheater combustor would be necessary to reduce the overall system pressure drop. A larger blower was ordered and has been delivered to DDA. The rework of the preheater combustor and the installation of this blower should be accomplished in the near future.

Test

All combustor testing during this reporting period was conducted after the installation of the high-temperature preheater. The combustor used during this series of tests consisted of the metal prechamber that had been used in all previous tests, the ceramic body and dilution band used in the initial ceramic durability test, and a new ceramic exit flange. The metal dome from the initial low-temperature Mod I combustor was used in this buildup and was instrumented with two embedded thermocouples so that its temperature could be accurately monitored. The combustor was initially operated with the rebuilt fuel manifold and its detached cooling tubes. Forty data points were recorded with this combination of components over a range of BITs from 857°C to 945°C (1575°F to 1733°F).

Several important observations were made during these tests. First, a source of ignition was not required to initiate combustion at these BITs. Neither the pilot flame nor the igniter was used, but combustion was quickly observed after the fuel was introduced to the high-temperature air. Second, since auto ignition could take place, lean blowout did not occur, and combustion was continuous regardless of the fuel/air ratio. Third, automatic ignition did not occur in the prechamber.

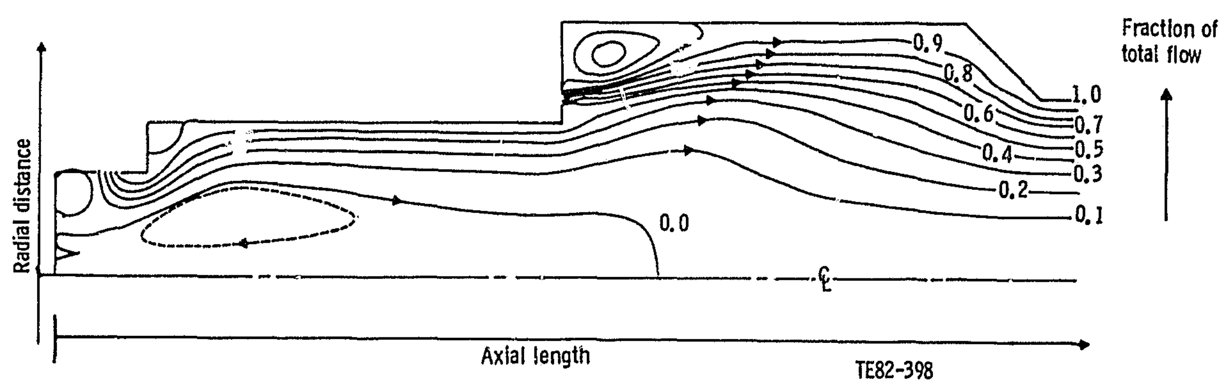

Figure 20. Concept 4 alternate combustor design—96 km/h (60 mph) flow streamlines.

Flashback into the prechamber was not a problem for burner inlet temperatures below 946°C (1734°F) as long as the variable geometry remained reasonably open. Fourth, the variable geometry was moved without difficulty at these high inlet temperatures after it had been properly aligned.

The emission results for these initial high inlet temperature tests were encouraging. The level of CO remained about the same as in earlier testing at 530°C (1200°F) BIT; however, the NO_X emissions were decreased by almost an order of magnitude. A serious problem was encountered with the operation of the main fuel nozzle manifold. Excessive manifold temperatures were observed as the BIT approached 860°C (1700°F), and these caused the fuel to vaporize within the manifold. Once vaporization occurred, a cycle was started in which fuel flow was temporarily reduced, allowing more fuel to be vaporized. Fuel supply pressure then increased, causing a surge of liquid fuel and a temporary reduction in manifold temperatures. When the manifold returned to its original elevated temperature, the cycle repeated. With each cycle, the fuel supply pressure surged approximately 69 kPa (10 lb/in.^{2}) and was accompanied by an observable blue flash in the combustor primary zone.

To reduce the problem of fuel vaporization, a new manifold was designed with improved cooling. The new manifold reduced the contact between the fuel and the hot prechamber wall and provided additional protection for the fuel by employing a quasiconcentric-tube heat exchanger. When the new fuel manifold was tested, fuel temperatures remained below 93°C (200°F), the fuel supply pressure and flow were completely steady, and the appearance of the flame was both clear and steady. At a BIT of 999°C (1830°F), a variety of variable geometry positions that caused neither automatic ignition nor flashback into the prechamber was explored. Flashback was intentionally induced by excessively closing the variable geometry mechanism and thereby increasing the residence time and fuel/air ratio in the prechamber.

Figure 21 presents the emission data obtained at 999°C (1830°F) BIT along with the results at 871°C (1600°F) and 627°C (1160°F). Each of these sets of data are for approximately equal burner outlet temperatures, and the lines shown represent movement of the variable geometry. At 999°C (1832°F), emission levels were below any value ever measured at DDA for previous AGT combustors, and NO_X is at a level near the accuracy limits of the measuring equipment.

It can be seen that at the lowest BIT tested (627°C [1160°F]), the emissions were well below the program goals. As the inlet temperature increased, however, the burner was capable of sustaining combustion at leaner fuel/air ratios. Thus the NO_X emissions could be decreased by lowering the flame temperature without a substantial change in CO emissions.

At a BIT of 999°C (1832°F) the measured NO_X emissions for these steady-state rig tests were almost two orders of magnitude below the program goal. At the same BIT but at a different variable geometry setting, the measured CO was 30 times below the program goal. Including both metal and ceramic AGT 100 combustor testing, a total of 37 burning hours have been accumulated and 192 data points have been recorded to date during this development effort.

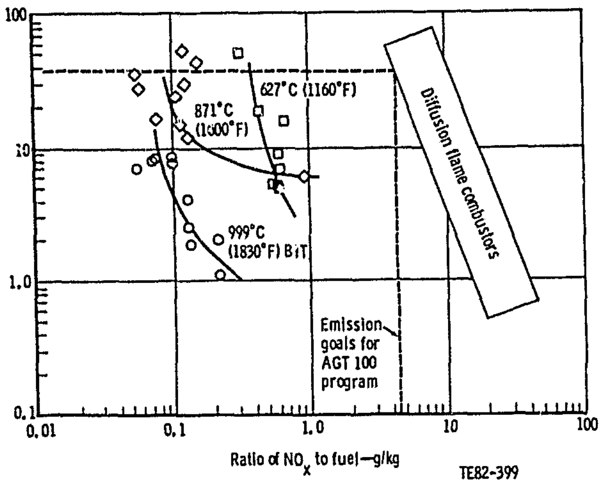

Figure 21. Combustor rig test emission results, 37 burning hr.

Ceramic Components

The ceramic dome (swirl plate) was redesigned to include stress relief slots between the inner diameter and the bypass holes. An existing dome was reworked to this latest design configuration by machining these slots with an ultrasonic impact grinder. A photograph of the reworked dome is shown in Figure 22.

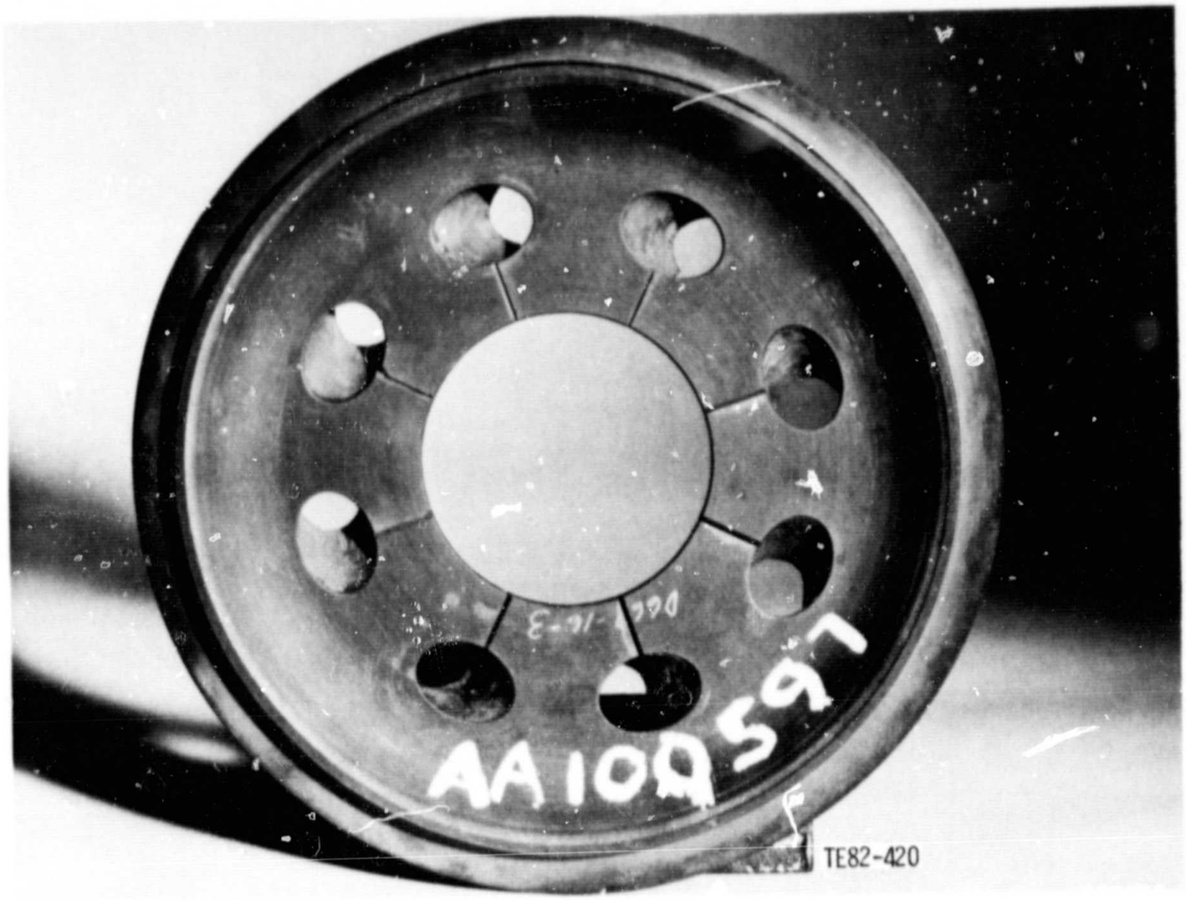

Figure 22. Ceramic combustor swirl plate (dome).

ORIGINAL PAGE
BLACK AND WHITE PHOTOGRAPH

VII. Regenerator Development

7.1 Reference Power-Train Design

Design work was completed on the regenerator cover and the ceramic exhaust duct/regenerator seal platform during this reporting period. These designs are being used in the Mod I engine with only minor changes. The general arrangement of the RPD regenerator system is shown in Figure 23.

Regenerator Cover

The detail design of the fabricated sheet metal regenerator cover for the AGT 100 engine was completed except for the air distribution manifold insert. This insert is required to match the regenerator air side distribution to the gas side distribution footprint. The cold flow air distribution model was redesigned to match the internal flow contours of the regenerator cover and was released for fabrication. The testing to define the manifold design is planned for early 1982. A test fixture was also designed to pressure test the cover and to determine the deflection characteristics under load.

Cold flow testing of the cover to model the regenerator air side flow path will be aimed at matching the gas side velocity (and corresponding flow) distributions discussed later. Emphasis will be placed on providing a flat distribution at cruise conditions with the objective of maximizing engine/driving cycle fuel economy.

Ceramic Exhaust Duct/Regenerator Seal Platform

The one-piece ceramic (LAS) exhaust duct/seal platform provides the flow transition from the power turbine exit to the regenerator gas side inlet and also the platform for the regenerator inboard seal. After several iterations, a design was completed that reduced predicted stresses and deflections to acceptable levels. A finite element model of this design is shown in Figure 24, and the resulting deflection predictions are depicted in Figure 25 when the part is loaded with a 344.8 kPa (50 lb/in.²) pressure differential. The predicted adjusted average stress level for this configuration was ≤ 27.6 MPa (4000

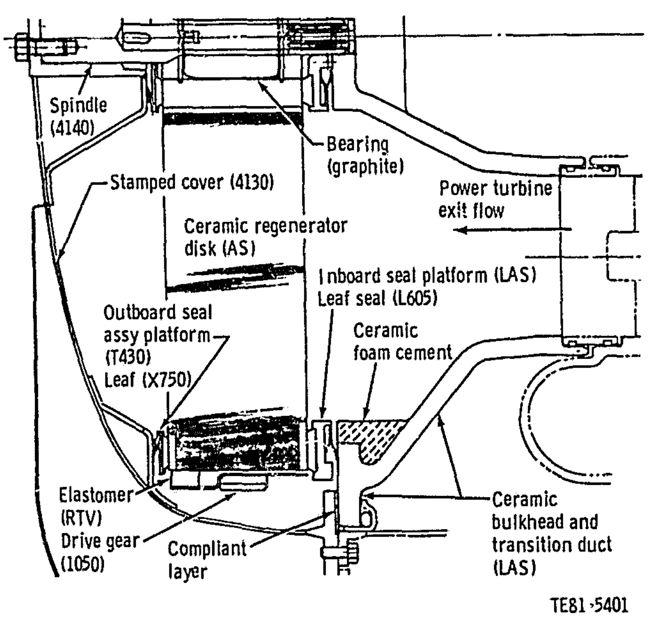

Figure 23. RPD regenerator seal development.

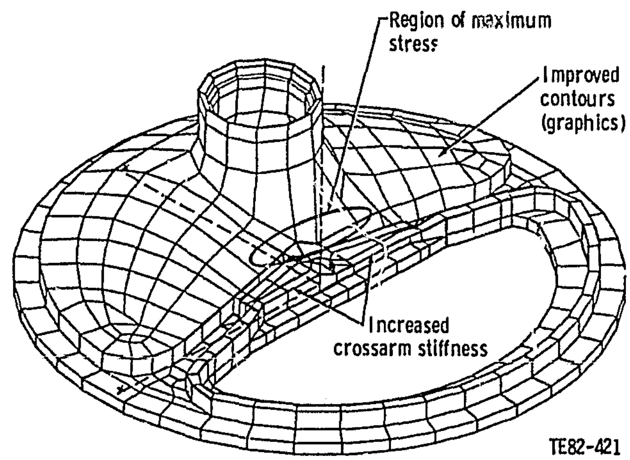

Figure 24. Finite element model of ceramic duct/seal platform.

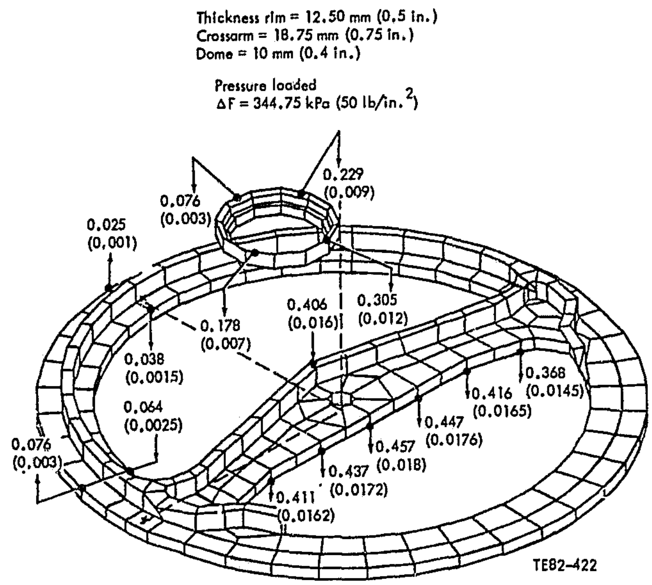

Figure 25. Calculated deflection distributions of ceramic exhaust duct/seal platform.

ORIGINAL PAGE IS OF POOR QUALITY

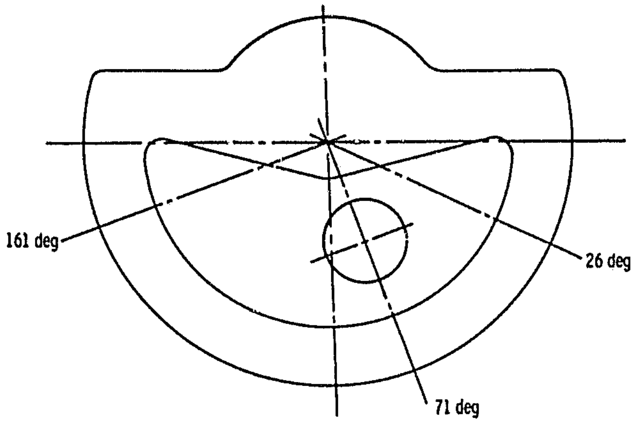

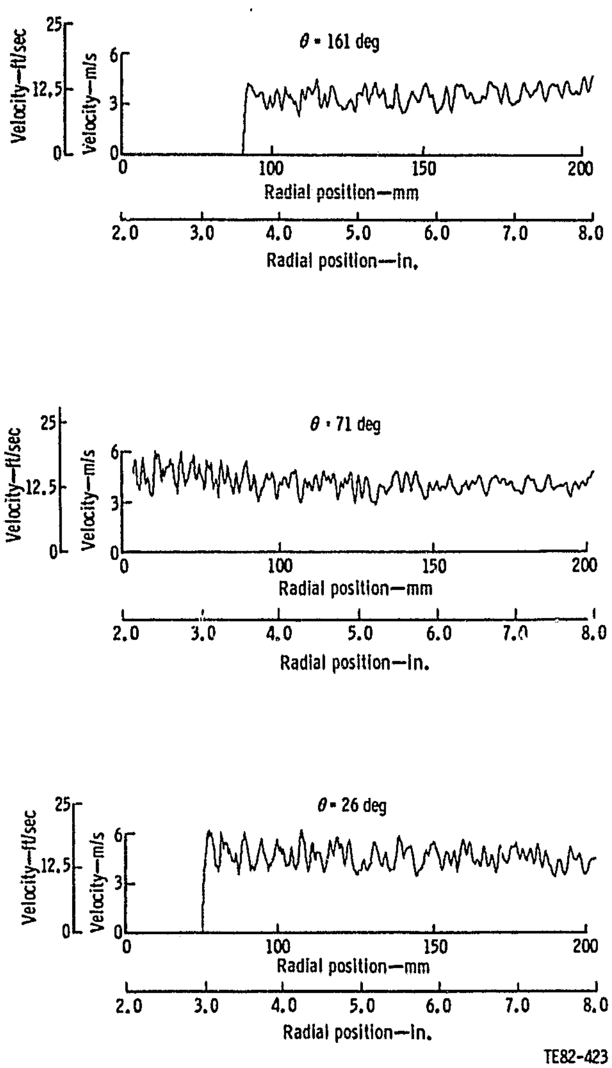

Figure 26. Regenerator gas side cold flow distributions at 30 mph cruise conditions (Configuration 1).

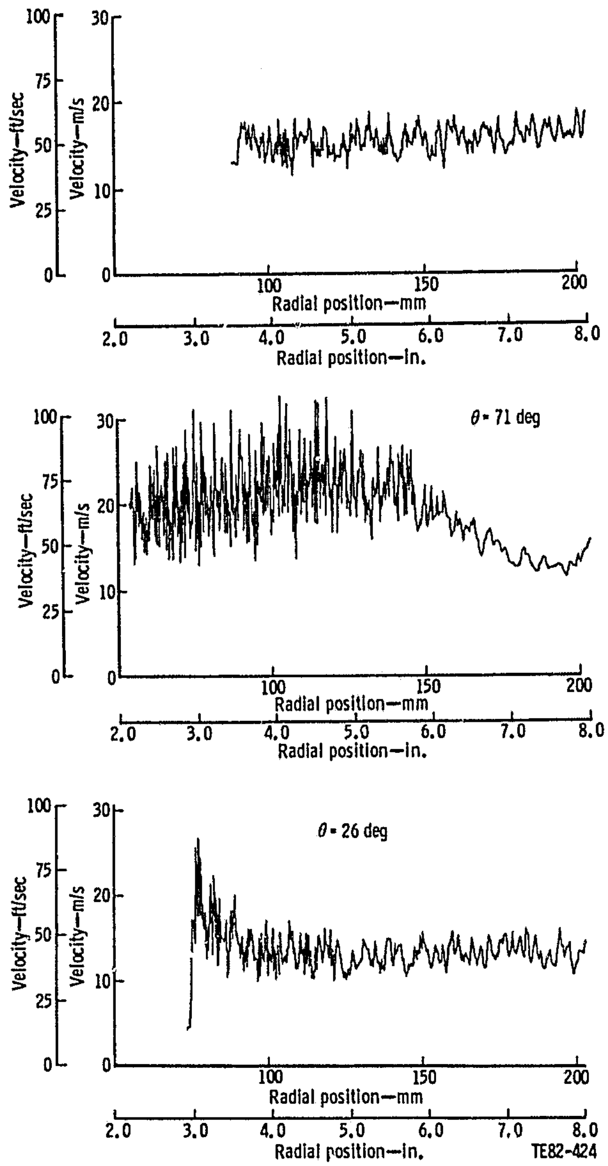

Figure 27. Regenerator gas side cold flow distributions at maximum power (Configuration 1).

lb/in.2) and the calculated failure rate was 1 in 925. The detail design of this configuration was completed and a model fabricated by Corning Glass Works (CGW) to study casting methods for the part.

The flow characteristics of this transition duct were evaluated using a cold flow distribution model that duplicated the duct/disk geometry and simulated the flow characteristics by modeling both Mach Number and Reynolds Number into the regenerator disk. Figures 26 and 27 illustrate the cold flow velocity distributions for the regenerator gas side flow path at the 48 km/h (30 mph) cruise and 100% power conditions at various circumferential positions around the duct. It should be noted that the velocity distribution is acceptably flat at the 48 km/h (30 mph) condition, whereas at 100% power there is a local peak in velocity in the vicinity of the power turbine exit. As noted earlier, comparable testing is to be completed to contour the regenerator cover air side manifold to match these gas side profiles.

ORIGINAL PAGE IS
OF POOR QUALITY

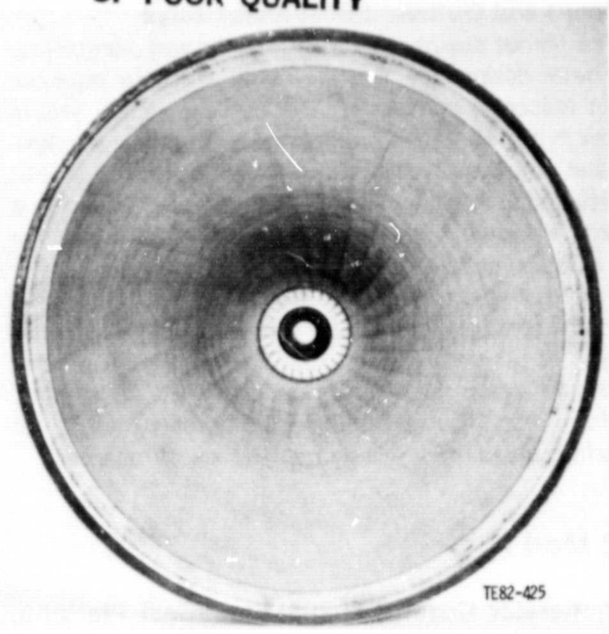

Figure 28. Regenerator disk after 100 hr test.

Disk/Ring Gear Assembly

The ceramic (AS) engine regenerator disk assembly is effectively the same as the current prototype disk under test and shown in Figure 28. A static load deflection test of this design has been completed and more than 100 hr of hot rig testing have been completed at conditions simulating 100% power with no problems encountered.

The present disk matrix is fabricated from CGW AS material with a maximum temperature rating of 1100°C (2012°F). Related material tests of this matrix indicated the deterioration of strength that occurs in the matrix if this maximum temperature is exceeded (see Figure 29). CGW is continuing work on a 1200°C matrix material that will be incorporated with the disk assemblies as it becomes available. Successful laboratory firing and testing of the 1200°C (2192°F) material has been conducted at CGW; work on converting these laboratory procedures into shop practice is now underway.

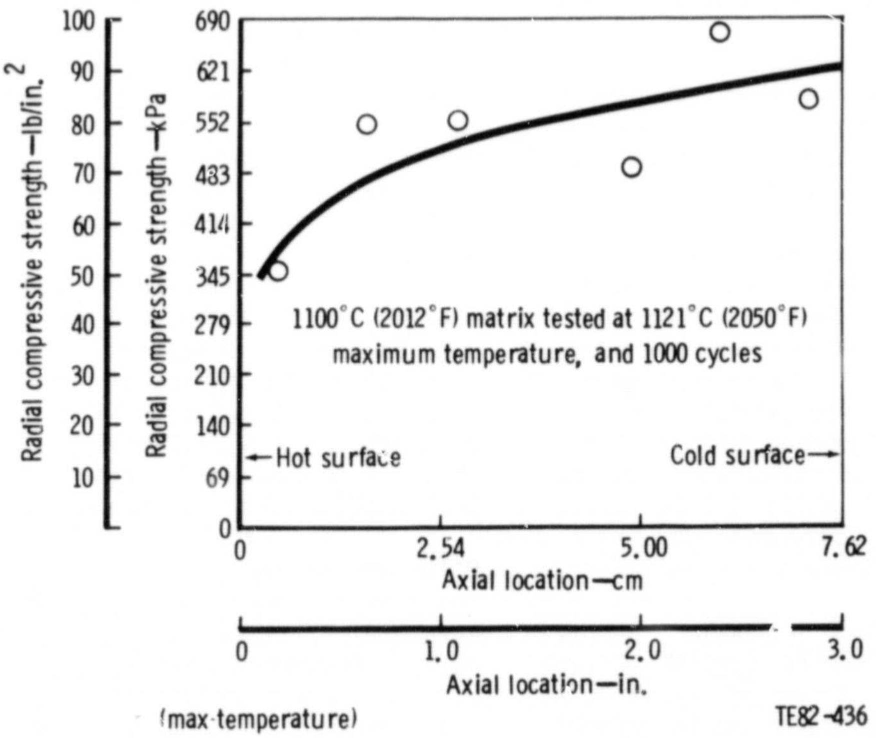

Figure 29. Strength properties of 1100°C (2012°F) AS disk material.

ORIGINAL PAGE IS
OF POOR QUALITY

Inboard and Outboard Seal Assemblies

The layout design of the RPD seals was completed, but detail designs were delayed until additional development testing is completed. The outboard (cold) seal is currently similar in design to the present prototype flexible leaf seal. Several alternate seal leaf designs have been completed to reduce cold seal leakages, and at least one alternate design is planned for preliminary testing within the next six months.

Two methods of wearface attachment to the ceramic inboard seal platform were under study. However, testing of several variable expansion coefficient plasma sprays to attach the NiO wearface to the LAS ceramic platform was unsuccessful, and the primary method for wearface attachment will be by mechanical means.

7.2 Mod I

Regenerator Cover, Exhaust Duct/Seal Platform, and Disk Assembly

With the exception of the inboard seal assembly, the Mod I regenerator system utilizes RPD components with only the minor modifications outlined below. Fabrication progress is also noted.

- Regenerator cover—addition of a D-shaped spacer on the outboard seal track to reposition the regenerator disks because of a thinner inboard seal assembly. A machined slot is added to the flange to prevent inboard seal rotation, and the disk spindle is modified to accommodate the repositioned disk. Fabrication of the cover and its pressure/deflection test fixture is proceeding on schedule with late February delivery expected. Deflections under simulated load will be measured to determine seal and disk operating geometry. If necessary, cover modifications will be made prior to engine build.
- Ceramic exhaust duct/regenerator seal platform—minor changes to the seal platform to remove an antirotation pin required for the RPD inboard seal A model of this part, shown in Figure 30, was made at CGW to develop the casting technique for this piece. The first successful castings have been completed at CGW, and final machining has been started. The first test piece is scheduled for completion in late January. A static test fixture has been designed and is being fabricated to conduct load/deflection testing of the ceramic duct/platform to verify component integrity and to compare actual characteristics to the finite element model predictions.
- Disk/ring gear assembly—no change in the configuration but 1100°C (2012°F) rated AS used in the disk. The ceramic disks have been completed by CGW and are being assembled with the ring gear at Harrison Radiator Division, General Motors Corporation. First delivery is expected by late January.

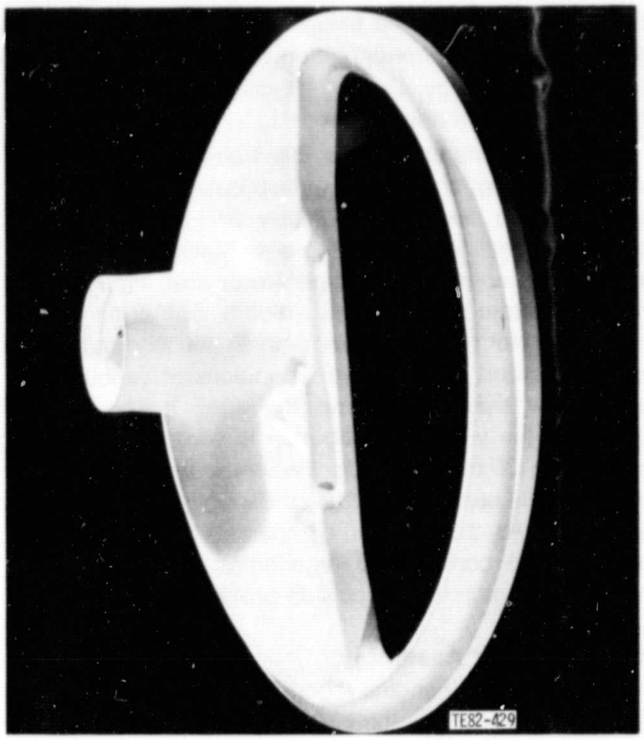

Figure 30. Model of ceramic exhaust duct/seal platform.

Inboard and Outboard Seal Assemblies

The lower operating temperature of the Mod I engine allows use of a conventional metal platform inboard seal assembly. The Mod I inboard seal design is of three-piece configuration and is based on similar designs tested in the DDA/CATE program. The rims, prestrained on assembly at room temperature, are designed to have minimal radial stress gradients at operating temperatures. This design reduces the coning effect that normally occurs. The crossarm platform is 2.5 mm (0.100 in.) INCO 625 to provide flexibility, and the wearface is a 90/10 composition of NiO/CaF_2 that has been successfully tested in the CATE program under similar operating conditions.

The seal/disk configuration for Mod I is shown in Figure 31, which illustrates the general seal leaf arrangement. Blockage of flow into and out of the disk has been minimized, and the configuration uses the same leaf retainer, hinges, and graphite components for both the inboard and outboard seals to minimize the tooling requirements for fabrication. Seal fabrication is being completed at HRD, and the first seals are expected in March.

Prototype Testing

Over 100 hr of testing have been accumulated on prototype AGT 100 regenerator components in the hot test rig at simulated Mod I operating conditions. The following tests have been conducted:

- base-line testing of one set of prototype regenerator hardware to determine performance characteristics

ORIGINAL PAGE IS
OF POOR QUALITY

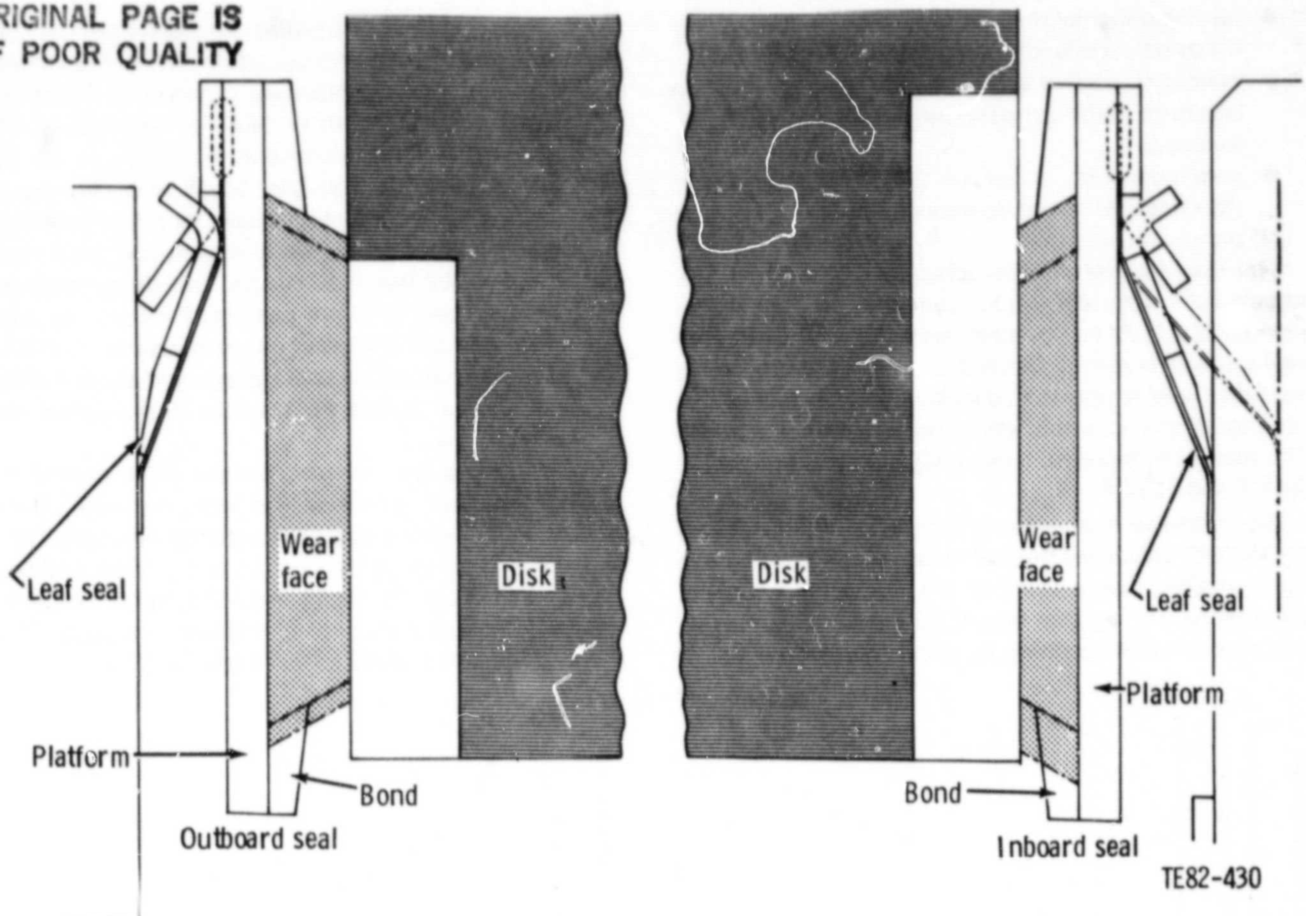

Figure 31. Mod I seal/disk configuration.

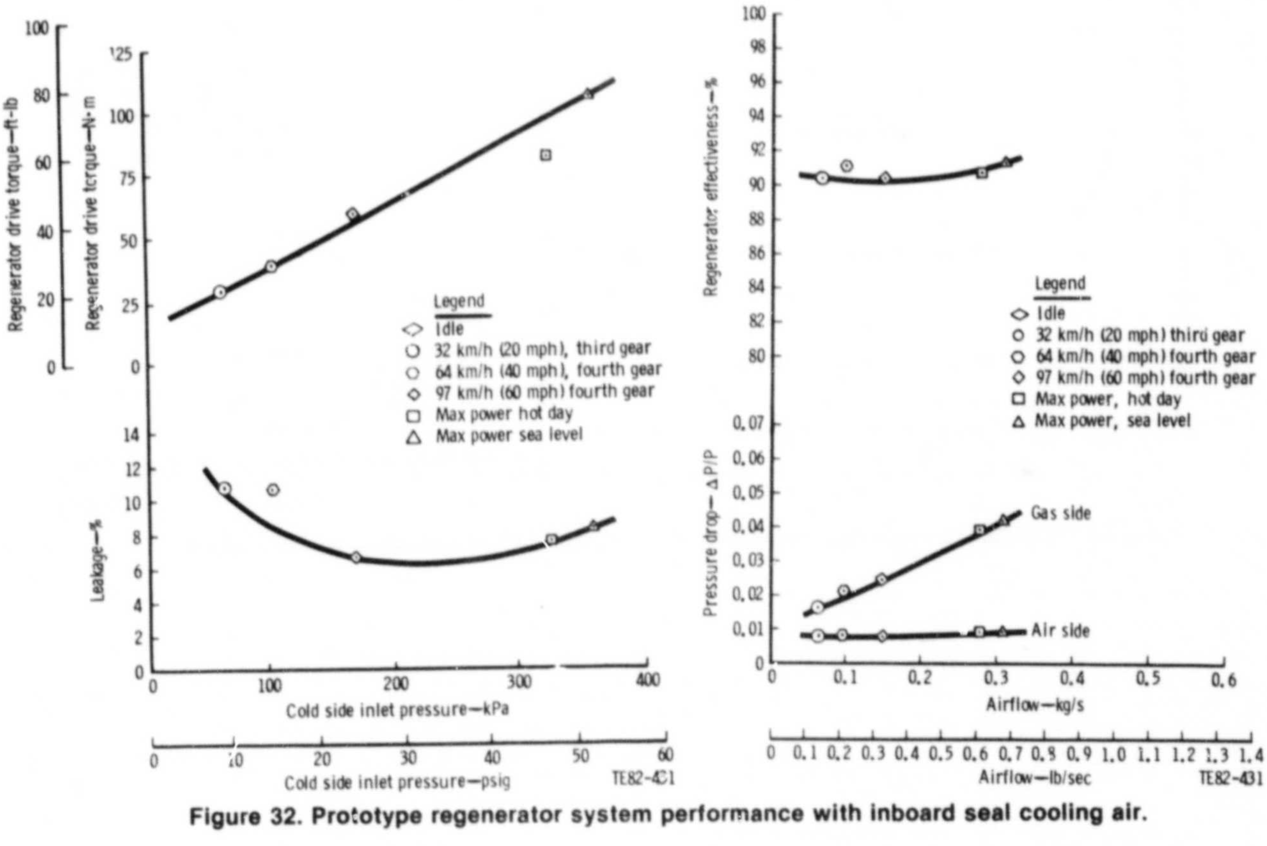

Figure 32. Prototype regenerator system performance with inboard seal cooling air.

- rig instrumentation and operational changes to minimize rig effects on regenerator performance
- effects of inboard seal crossarm cooling levels on crossarm metal temperatures and regenerator performance
- parameter tests at various T_6 levels to determine the effects of operating temperature on regenerator performance

The resulting performance characteristics of the prototype AGT 100 regenerator systems are depicted in Figures 32 and 33 for operation with and without inboard seal crossarm cooling. Inboard seal metal temperatures recorded with temperature-sensitive paint indicated that cooling airflow had little effect on metal temperatures. The maximum recorded was between 840°C and 890°C (544°F and 1634°F).

Rig-measured regenerator effectiveness (air side) was consistently calculated below the expected values for this configuration. Examination of the rig and subsequent calculations verified that significant blockage of the gas side disk rim was occurring from the combined effect of the rig flow path liners (to protect rig walls from high gas temperatures) and the undersized rim I.D. of the inboard seal platform. These blockages, outlined in Figure 34, were subsequently shown to cause an estimated 1.3% reduction in disk effectiveness at maximum power but only a negligible effect at idle. Study is continuing on these rig-to-engine correlation values for this regenerator.

A second set of prototype hardware has been completed and will be tested in January. seal design changes have reduced seal crossarm platform thickness for additional flexibility and increased crossarm damping. The effect of these changes on seal leakage and system effectiveness will be studied for possible incorporation into engine hardware.

A design change has been completed to modify the hot rig to accept Mod I engine seals and disk. These modifications will be completed during February 1982, and the rig will be operational to test engine hardware sets in March. Limited rig testing will then be conducted to qualify engine sets and to evaluate design/development changes to the AGT 100 regenerator.

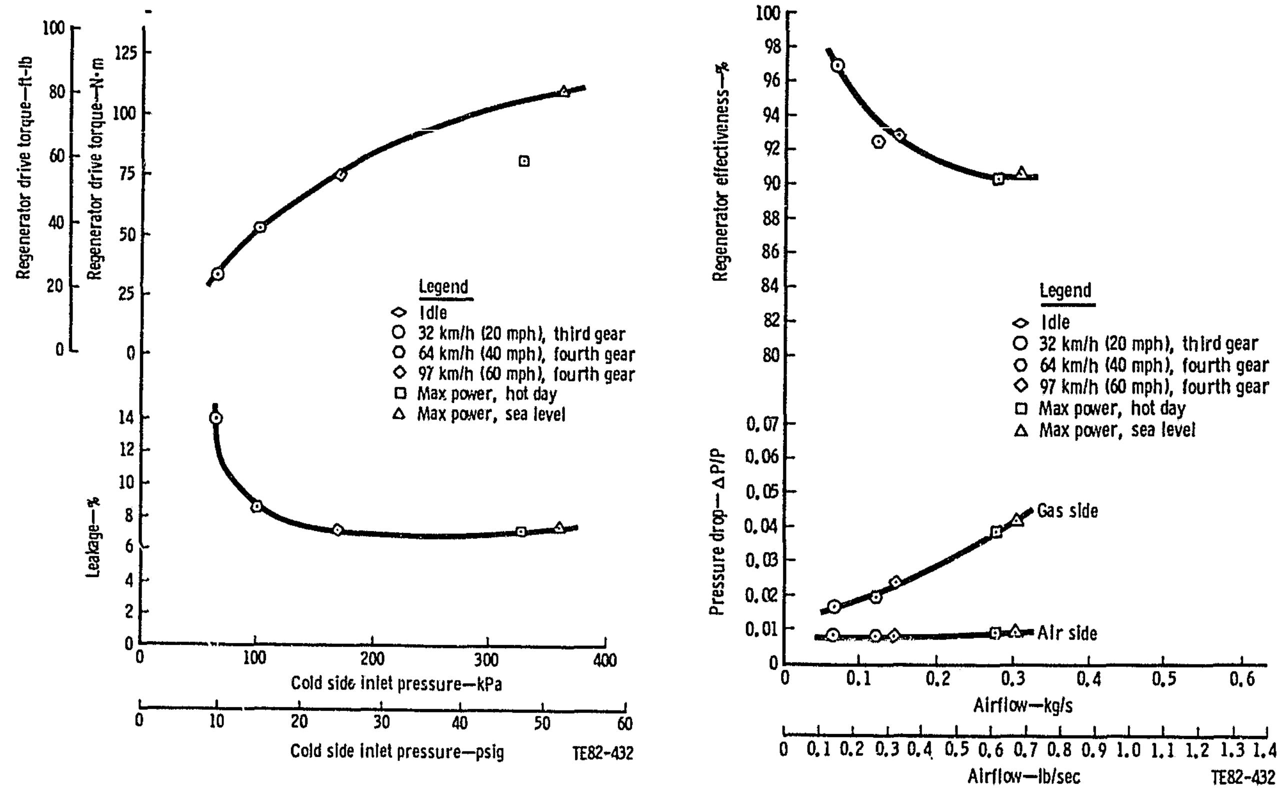

Figure 33. Prototype regenerator system performance without inboard seal cooling air.

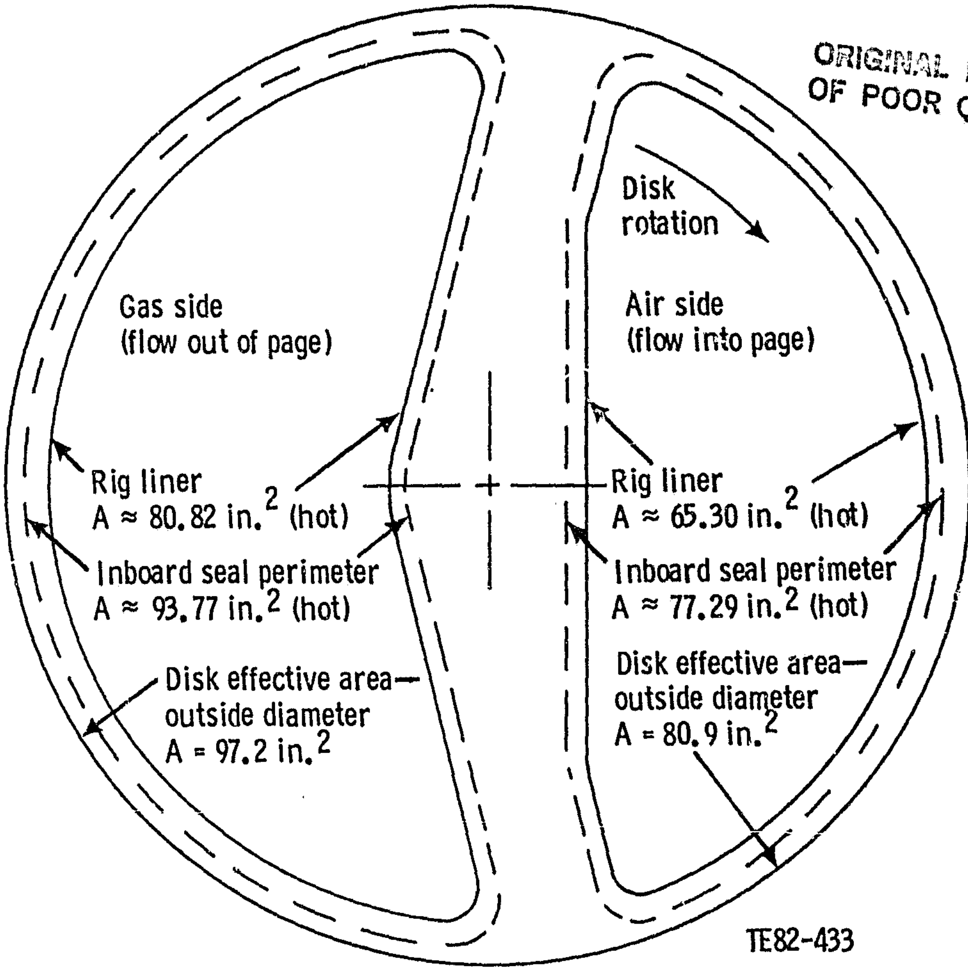

Figure 34. Regenerator disk blockage due to rig liner and inboard seal.

8.1 Structures

Structural design work was completed on the combustion case assembly, insulation, ceramic and metal scrolls, and the Mod I engine limit stack.

Combustor Case Assembly

The combustion case assembly was previously referred to as the hot section housing. The name was changed to better describe the part function. The first two engine cases are being fabricated in AISI 410 material instead of AISI 4130 production material to reduce the risk of failure during initial testing. AISI 410 material is more costly and has higher strategic material content than AISI 4130 but also has increased high-temperature strength and does not require a corrosion resistance coating. This will provide greater safety during the evaluation of the insulation material and case metal temperature.

Insulation

Johns Manville Cerachrome and Min-K insulation were selected to be evaluated in the first Mod I engine program. The entire insulation package contains 23 pieces that are installed in a sequential order during the engine build. The resulting assembly is firmly locked in place between the combustion case wall and the engine components.

Babcock & Wilcox Unifelt 3000 material is still being considered for evaluation during later engine development testing.

8.2 Gearbox and Power Transfer

The layout describing the simplified gear train was completed along with detail drawings of the component parts. Figure 35 and Table IV show the general arrangement and pertinent parameters of the gear train.

The power transfer clutch inner cone facing material has been changed from paper-based to fluorocarbon-based friction material. This occurred when the original material, Borg-Warner SD-1799L, became unavailable for this application. The new material, Garlock Grylon®, has been used satisfactorily in similar applications by this division.

Alternate bearing suppliers have been selected for all main shaft bearings.

8.3 Starter/Boost System

The starter drive is integral to the gasifier rotor gear train and drives the starter continuously during engine operation. When starter torque is required to assist in "spooling up" the gasifier rotor or to start the engine, the brushes are dropped against the commutator.

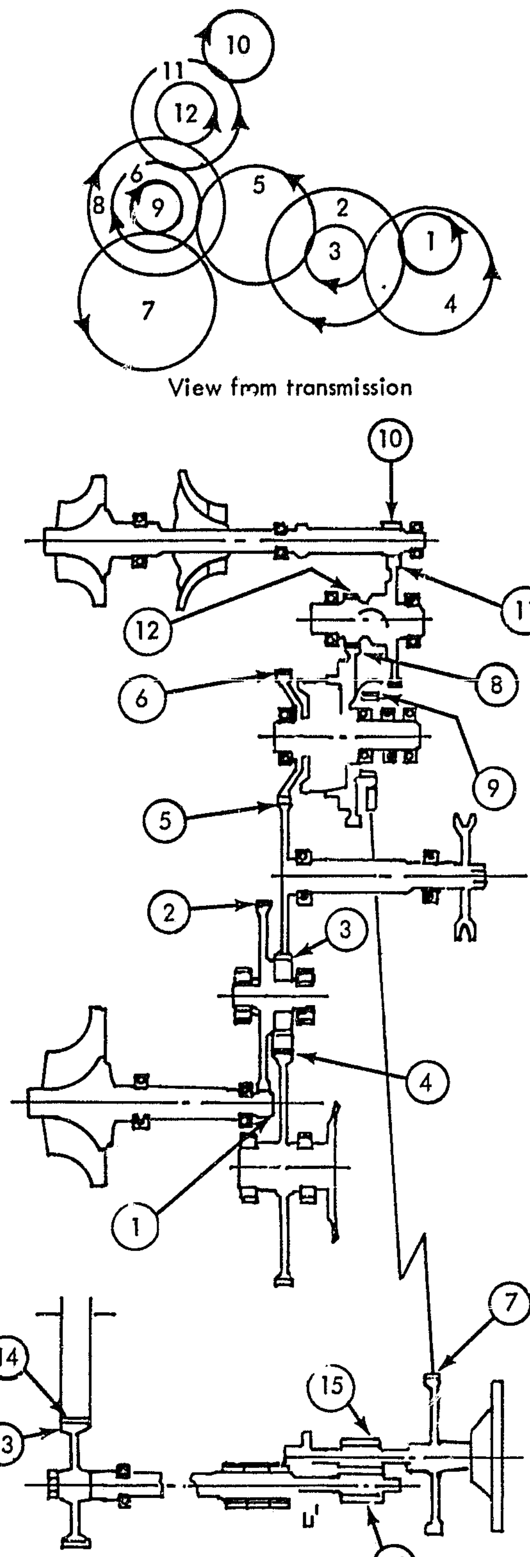

Figure 35. Gear schematic.

Cycling endurance tests were conducted to determine the best brush composition available to withstand the high current and rapid cycling as anticipated in actual operation.

The best brush durability to date has been achieved with the standard 27MT motor brushes. These consist of 95% copper and 5% other materials, such as graphite and iron. Tests extended to 70,000 one-second cycles, with a maximum wear of 4.57 mm (0.18 in.). Allowable wear can approach 7.62 mm (0.30 in.). It is probable that one brush change will be needed to complete the 152,000 cycles anticipated in use. Stackpole will furnish a higher metal content that will be tailored to this particular requirement. Testing will be conducted on these brushes as soon as they are received.

Brush lifting mechanism durability tests were also conducted. The assembly tested included the lever, cams, rollers, and brush holders. Durability testing was stopped after completion of 250,000 cycles, and parts were examined for wear. No significant wear was observed, although the brush holder bearing pins were slightly grooved. These will be further hardened and perhaps chrome plated if necessary.

Due to the difficulty of insulating the brush holder and positive brush from both the frame and lifting mechanism, the positive brush was insulated from its brush holder by a high-temperature glass, Nomex insulation. Also, the positive lead brush attachment screw was insulated from the brush holder with a mica-filled washer. These changes reduce accidental electrical damage and simplify construction while retaining much of the heat sink function of the brush holder.

Casting drawings and long lead parts were sent to the model shop in September, while all parts were in process by mid-October. Thus, parts for a complete motor should be available in February, and delivery of this first motor is planned shortly thereafter, following performance testing and brush seating cycling tests.

Table IV. General gear train arrangement.

Gear	Function	Teeth	Module	Helix	100% rpm	Material
1	Power turbine	21	1.25	20°L	53395	9310
2		120	1.25	20°R	9344	9310
3		38	1.75	0	9344	8620
4	Output	116	1.75	0	3061	8620
5	Accessory drive	78	1.75	0	4552	8620
6	N_2 clutch	63	1.75	0	5636	8620
7	Starter	77	1.75	0	3074	8620
8	N_1 clutch	88	1.75	0	5636	8620
9		42	1.75	0	5636	8620
10	Gasifier	21	1.25	20°L	86256	9310
11		84	1.25	20°R	21564	9310
12		23	1.75	0	21564	9310
13		86	1.25	0	102.5	1141
14	Regenerator	392	1.25	0	22.49	1050
15	Oil pump	8	3.175	0	3074	8620
16	Oil pump	8	3.175	0	3074	8620

ORIGINAL PAGE IS OF POOR QUALITY

IX. Materials Development

9.1 Thermal Barrier Development

The primary structural ceramic material in the RPD engine is silicon carbide. To obtain optimum engine performance it is necessary to operate at high temperature—in the range of 1288°C (2350°F). Since silicon carbide has a high thermal conductivity, steps must be taken to reduce heat transfer to the surrounding structures. It is necessary, therefore, to introduce thermal barrier materials in strategic locations to prevent excess heat loss from the engine and to maintain structure temperatures within acceptable operating ranges. Candidate thermal barrier materials need to have low conductivity, adequate strength, compatible thermal expansion coefficients, and the capability of being produced in proper shapes and sizes.

Several materials have qualities that make them suitable candidates—mullite, cordierite, zircon, and zirconia are the primary possibilities. Table V lists typical thermal properties for these four materials.

Table V. Thermal properties of candidate thermal barrier materials.

	Average CTE · 10^{-6}		Thermal conductivity	
Material	**per °C**	**per °F**	**W/m·K**	**Btu/hr·ft·°F**
Mullite	4.5-5.7	2.5-3.2	5.5	3.17
Cordierite	1-2	0.5-1	1.7-4.2	0.97-2.4
Zircon	3.7-6.2	2.1-3.4	5.0	2.9
Zirconia	9.5-10.5	5.3-5.8	1.8	1.05

Thermal barrier components are required in a variety of shapes. Materials have been investigated that can be formed by either hot pressing or standard pressureless sintering techniques. Hot pressed materials offer high strength and elevated temperature stability and are attractive as a means of diffusion bonding composite structures. However, hot pressing is generally limited to making simple shapes. Pressureless sintering opens up the possibilities for larger and more complex shapes and generally is more cost effective.

Of the materials listed in Table V only zirconia is commercially available as a high-strength structural material. The other three are used widely as heavy refractories for glass and steel processing and are not readily available in high-purity high-density forms.

CBO has embarked on a program to develop both hot pressed and sinterable mullite/cordierite as a joint material to attach the SiC rotor to the metal shaft. DDA concurrently initiated work to develop zircon-based materials. Zirconia has been supplied for developmental studies by both Kyocera International and the AC Spark Plug Division of GM.

The following three subsections describe the progress to date in the development/evaluation of these materials.

Carborundum Effort

CBO is developing procedures to make mullite/cordierite materials by hot pressing and pressureless sintering. The goal of this program is to produce materials that have a net coefficient thermal expansion (CTE) equal to silicon carbide (1.74×10^{-6}). The goal for this reporting period was to produce initial materials and obtain quantitative CTE data.

POWDER PREPARATION

Experience has shown that sol-gel prepared powders are more effective than pure oxide powders. Sol-gel techniques have helped to produce high-strength materials of higher purity than can be produced by using naturally occurring minerals. These techniques have helped to extend the applicability of fundamental ceramic systems such as mullite and cordierite.

Sol-gel procedures consist of a sequence of (1) solution, (2) coprecipitation, (3) drying, and (4) comminution. Compounds containing the metallic ions are dissolved in a common solvent. Precipitation is then promoted by altering the ph of the solution and thereby producing fine high-purity crystalites. This procedure creates an intimate mixture of the metallic ions and produces a more reactive powder. Optimum densities are therefore more easily attainable during sintering with these powders.

HOT PRESSED MULLITE/CORDIERITE

Hot pressing was performed by pressing the sol-gel powders in a graphite die heated by induction. Powders were designated as two component (calcined mullite and cordierite) and one component (uncalcined). The two-component powders were prepared by mixing precalcined mullite and cordierite. The end members were prepared by sol-gel techniques to yield stoichiometric mullite ($3Al_2 \cdot 2SiO_2$) and cordierite ($2MgO \cdot 2Al_2O_3 \cdot 5SiO_2$). The one-component powders were prepared in one step to yield various ratios of mullite and cordierite after *in situ* reaction.

Disks were made from each powder using a standard time/temperature/pressure schedule while varying composition. Table VI lists the measured density and CTE results for the hot pressed materials. Figure 36 illustrates the CTE data for the hot pressed materials.

PRESSURELESS SINTERING OF MULLITE/CORDIERITE

Agglomerated powders have been prepared with additives to facilitate forming. The powders were then formed to shape by classical uniaxial die pressing techniques. The shrinkage and density have been measured for several powder systems, as shown in Table VII. The theoretical density results are very significant and illustrate that high-density/low-porosity materials can be fabricated by pressureless sintering techniques.

ORIGINAL PAGE IS
OF POOR QUALITY

Table VI. Hot pressed mullite/cordierite—density and CTE data.

Composition—% cordierite*	Density—g/cm³ A	Density—g/cm³ B	Theoretical density—% A	Theoretical density—% B	CTE ·10^{-6} at 1300°C (2372°F) A per °C	A per °F	B per °C	B per °F
100%		2.63		104.0%			4.30	2.39
							4.23	2.35
							4.15	2.31
75%	2.75	2.69	103%	101.1%	4.23	2.35	4.40	2.44
					4.10	2.28	4.00	2.22
50%	2.72	2.85	96.9%	101.5%	5.07	2.82	4.90	2.72
					5.23	2.91	5.00	2.78
30%	2.42		80.7%		5.08	2.82		
					5.23	2.74		
					5.38	2.99		
25%		2.96		99.7%			6.40	3.56
							6.20	3.44
0%		2.30		73.0%			5.90	3.28
							5.84	3.24

*Balance is mullite
A = two-component powder, B = one-component powder

Table VII. Sintering data for mullite/cordierite powders.

Target composition—% cordierite*	Fired density—g/cm³ B	Fired density—g/cm³ A	Theoretical density—% B	Theoretical density—% A	Diametral shrinkage—% B	Diametral shrinkage—% A
75%	2.51	1.59	84.5	55.6	27.4	16.3
50%	2.42	1.52	86.2	54.7	27.6	1.4
30%	2.52	1.48	94.7	62.6	28.5	5.9

*Balance is mullite
A = two-component powder, B = one-component powder

In summary, materials have been produced using mullite and cordierite. Techniques have been developed whereby sol-gel powders are prepared and then used for hot pressing and pressureless sintering. Materials have been made ranging from 100% mullite to 100% cordierite, and CTEs were measured for these hot pressed materials. Compositions between 15% and 30% cordierite by weight (hot pressed material) are projected to have thermal expansion compatibility with silicon carbide. Further work will be centered on obtaining CTE data for sinterable bodies and for improving the density and consistency of the CTE data.

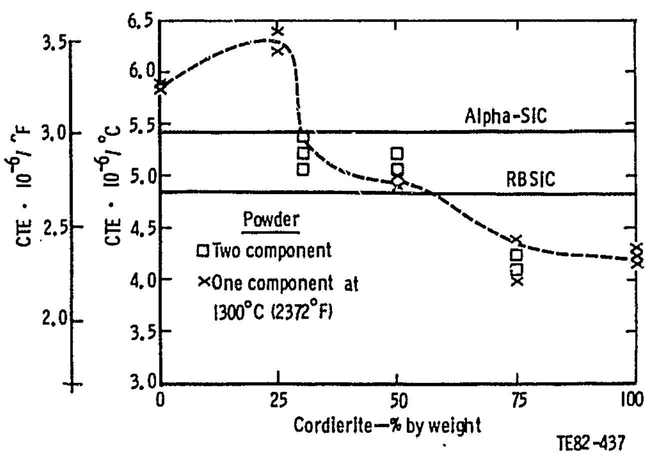

Figure 36. Coefficient of thermal expansion for hot pressed mullite/cordierite.

DDA Effort—Zircon

As a parallel effort, work was initiated at DDA to develop procedures for fabricating a sinterable thermal barrier material based on zircon ($ZrO_2 \cdot SiO_2$). Trial material systems are being studied to determine sinterability, expansion, strength, and microstructure.

Zircon is a naturally occurring mineral in the form of a sand and, as such, must be ball milled to yield a fine-grained sinterable powder. As a result, commercially available powders contain additional silica contributed by the flint grinding media.

Experiments were performed to evaluate shrinkage and densification in terms of some fundamental processing variables: (1) green compact density, (2) chemistry (sintering aids), and (3) firing temperature. A standard technique was developed for the preparation of all agglomerated powders. Compacts were formed by uniaxial die and isopressing techniques. Initial studies were performed with as-received zircon powders. Some preliminary work was accomplished with zircon/alumina and zircon/zirconia systems.

Uniaxial die pressed compacts were prepared to evaluate the effect of green density. Figure 37 illustrates the variation of apparent pore fraction and percent diametral shrinkage with green density.

Sintering aids may be useful to promote densification of the material at a lower temperature. Information in the literature indicated that particular oxides behave as sintering aids. Data in Table VIII illustrate that the firing temperature for a particular powder can be reduced and still yield a minimum pore fraction. The maximum attainable density is 4.21 g/cm^3, which is the theoretical density for zircon. The lower density is believed to be due to additional silica. To alleviate this problem, alumina and zirconia were added to react and form mullite and zircon respectively. Both approaches appear to be reasonable solutions. However, in both cases the pore fraction was increased—to 0.134 for zircon/alumina and to 0.075 for zircon/zirconia. Further effort will be directed to optimize the phase purity of these materials. The crystalline phase purity has a great impact on the percentage of expansion with temperature.

Figure 38 illustrates the expansion versus temperature for zircon and zircon/alumina. Of the two materials, the zircon/alumina exhibited the best match with SASiC. The greater expansion rate of zircon between room temperature and 250°C (482°F), as indicated by the dashed line, has been attributed to the expansion of cristobalite.

Polished sections were made for nominal microstructure evaluation. Figure 39 illustrates the microstructure for zircon. Some improvements in the pressing operation produced microstructures as shown in Figure 39. Figure 40 shows that the matrix is very fine grained with some extraneous free quartz. Figure 41 shows the microstructure for zircon/alumina. There is considerably more visible porosity in the latter material, as would be expected with a pore fraction of 0.134.

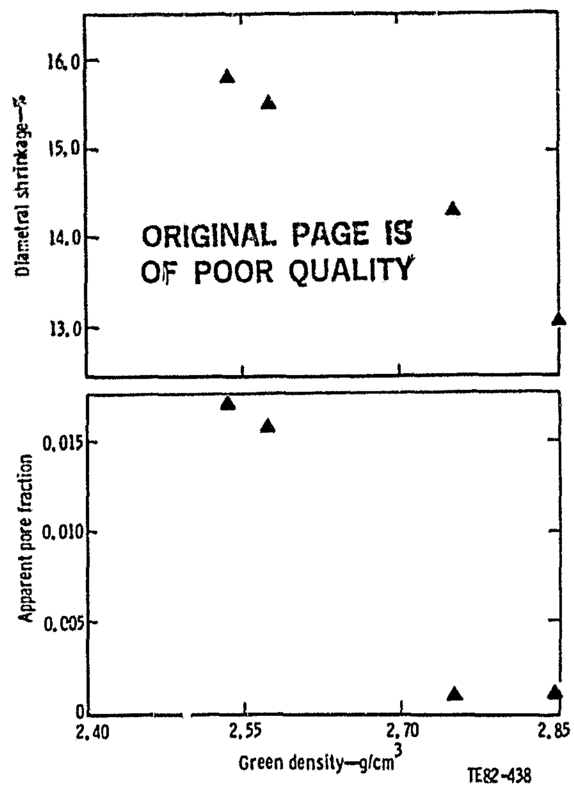

Figure 37. The effect of green density on the apparent pore fraction and percentage of dimetral shrinkage.

The strength and modulus data listed in Table IX were measured for materials representative of Figures 39a and 41.

The low strengths measured for these materials are believed to be due to the gross defects and porosity. Figure 42 shows that in both materials the fracture was initiated by an agglomerate just below the tensile surface. Figure 39a showed that this was typical for the entire material. Improvements were made, as shown in Figure 39b, to alleviate this problem.

In summary, pertinent ceramic processing variables have been determined for fabricating fine-grained, low-porosity zircon-based materials. Studies in powder compaction have helped to determine the optimum pressure

Table VIII. The effect of sintering aids on the apparent pore fraction.

Powder/additive	Apparent pore fraction at firing temperature T_1	T_2
As received	0.008	0.00017
As received plus additive A	0.0002	0.00001
As received plus additive B	0.0007	0.00035

* Based on the weight percentage of absorbed water.

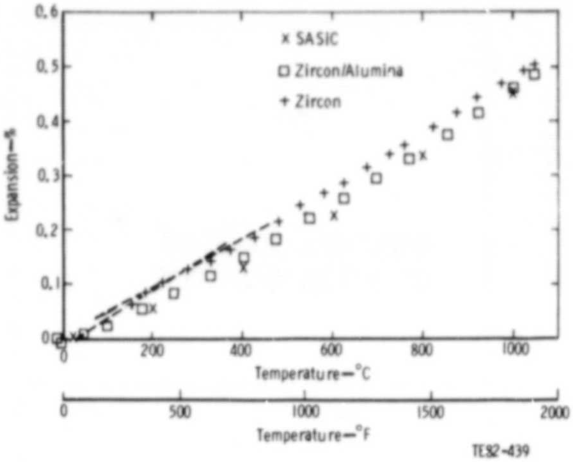

Figure 38. Expansion versus temperature for zircon and zircon/alumina.

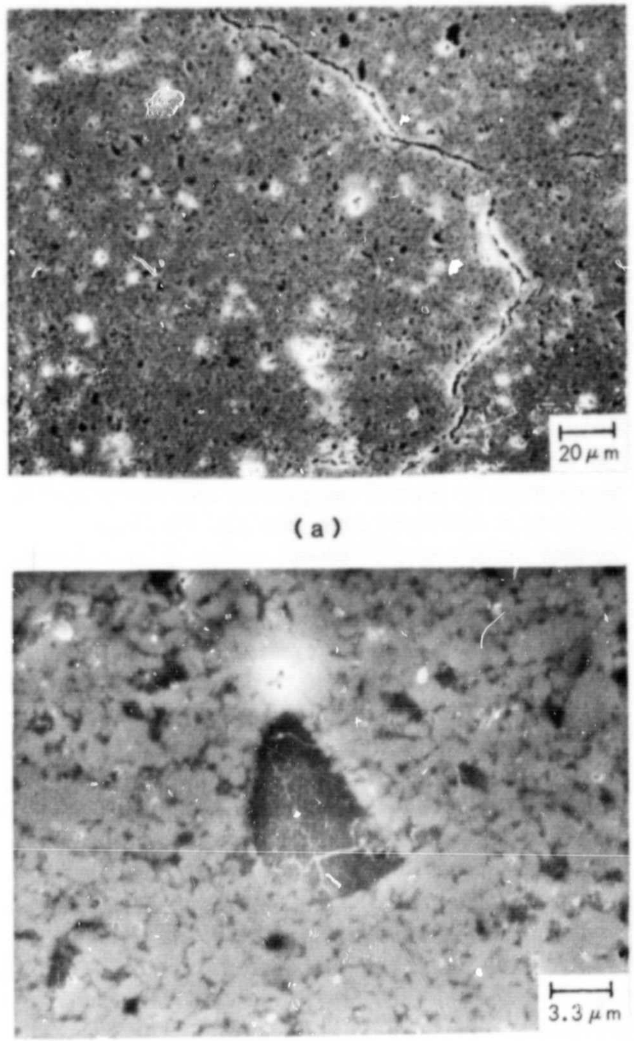

(a)

(b) TE82-1131

Figure 40. SEM micrographs of zircon.

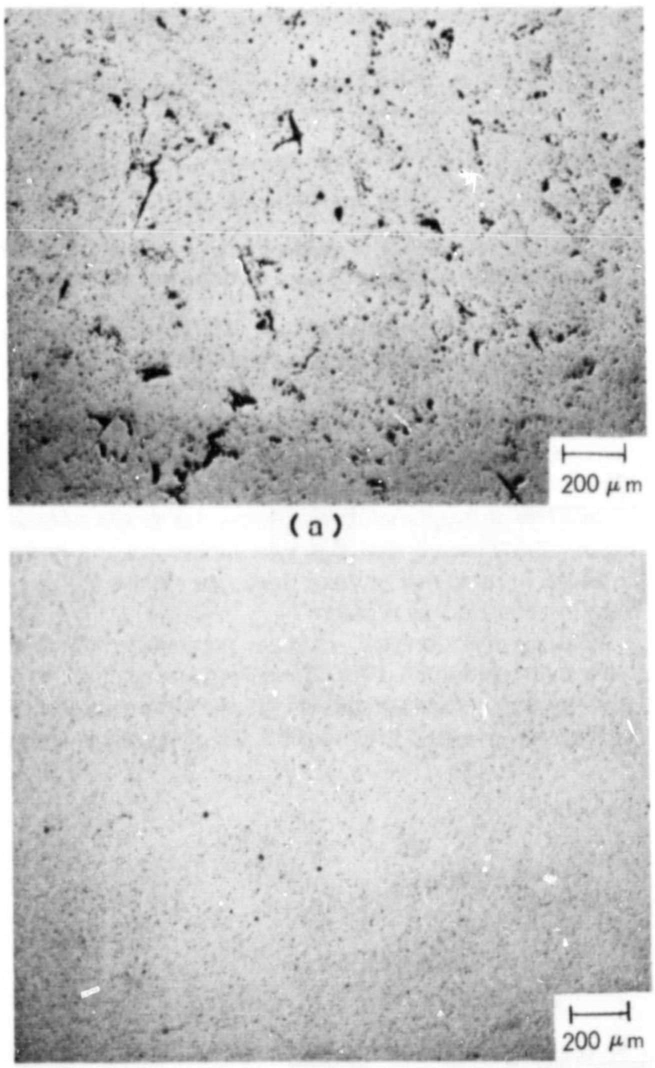

(a)

(b) TE82-1130

Figure 39. Zircon microstructures (a) early and (b) after pressing improvements.

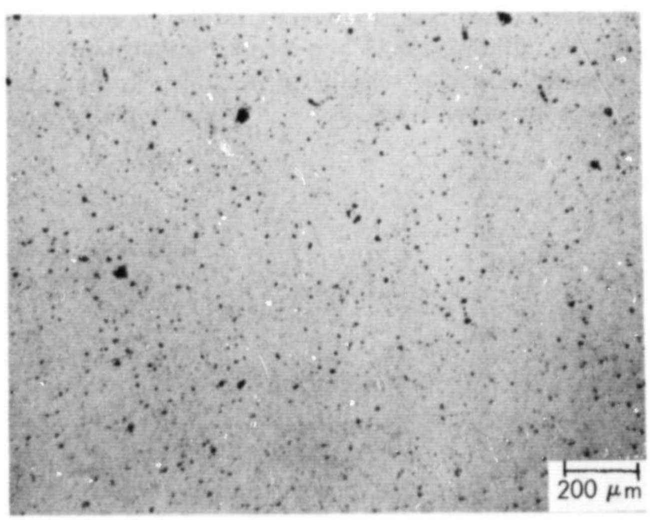

Figure 41. Microstructure for zircon/alumina.

Table IX. Strength and modulus data for zircon and zircon/alumina materials, with as-fired surface and at room temperature.

Material	Modulus of elasticity GPa	Modulus of elasticity 10^6 psi	Poissons ratio	Four-point bend strength MPa	Four-point bend strength ksi	Standard deviation MPa	Standard deviation ksi	No. of samples
Zircon	182.0	26.43	0.36	123.47	17.91	7.16	1.04	5
Zircon/alumina	174.8	25.35	0.42	128.50	18.64	13.16	1.91	7

for obtaining minimum porosity in a fired body. Two particular oxides have been found to assist in densifying fine-grained zircon. In conjunction with the two variables discussed above, the optimum firing conditions have been determined for several zircon-based bodies. In regard to thermal expansion, the zircon/alumina materials have been shown to possess ideal expansion characteristics for compatibility with SASiC.

According to the evidence provided here, zircon and zircon-based materials show good potential for thermal barrier applications. Future work will be directed toward optimization of the material strength along with measurement of the thermal conductive properties (diffusivity and specific heat).

DDA Effort—Zirconia

Zirconia is outstanding as a refractory material and is a very good thermal insulator. It is being considered as a thermal barrier material for applications in which thermal expansion compatibility is not required. During this period, materials have been received for evaluation from AC Spark Plug Division of GMC and Feldmuhle/Kyocera International.

Test bars have been received, and the strength data are listed in Table X. Representative micrographs illustrate the microstructures for these two materials, as shown in Figure 43. The AC Spark Plug zirconia has a finer grain size than that from Feldmuhle. The Feldmuhle zirconia has higher room temperature strengths. Figure 44 shows that there is not a direct fracture path in this material at room temperature. However, at high temperature the path of fracture is more discernible (see Figure 44). The strength of the AC zirconia is apparently controlled by processing-related defects. Figure 45a shows a circular pore possibly centered by a hollow spray dried agglomerate, and Figure 45b shows a subsurface pore that was also a fracture origin.

Of specific interest in the procurement of the thermal barrier materials are their expansion and heat conducting capacity (specific heat). Figure 46 illustrates the percentage of expansion with increased temperature for these materials. Both zirconias have considerably greater expansion than does Hexoloy® SA. The approximate CTEs between 800°C and 900°C (1472°F and 1652°F) are $5.5 \cdot 10^{-6}$/°C ($3.05 \cdot 10^{-6}$/°F) for alpha-SiC, $7.0 \cdot 10^{-6}$/°C ($3.9 \cdot 10^{-6}$/°F) for AC Spark Plug zirconia, and $12.5 \cdot 10^{-6}$/°C ($6.9 \cdot 10^{-6}$/°F) for Kyocera zirconia. Table XI lists the measured specific heats for these same materials.

Table X. Strength and elastic property data for AC Spark Plug and Feldmuhle zirconia.

Vendor/ Material	Modulus of elasticity GPa	Modulus of elasticity 10^6 psi	Poissons ratio at room temperature	Tensile surface condition	Temperature °C	Temperature °F	Four-point bend strength MPa	Four-point bend strength ksi	Standard deviation MPa	Standard deviation ksi	No. of samples
AC Spark Plug/ partially stabilized zirconia, 5.693 g/cm³	206.8	30.00	0.5	As received	Room temperature		315.0	45.69	15.7	2.27	4
				Machined	1000	1832	215.4	31.24	87.7	12.72	5
				Machined	Room temperature		343.3	49.79	22.9	3.32	6
Kyocera/ partially stabilized zirconia, 5.757 g/cm³	200.6	29.10	0.4	As fired	Room temperature		447.8	64.95	16.5	2.40	5
				Machined	Room temperature		539.8	78.30	36.1	5.24	5
				Machined	1000	1832	207.0	30.02	16.1	2.34	5
				Machined	1200	2192	156.6	22.72	17.4	2.53	5

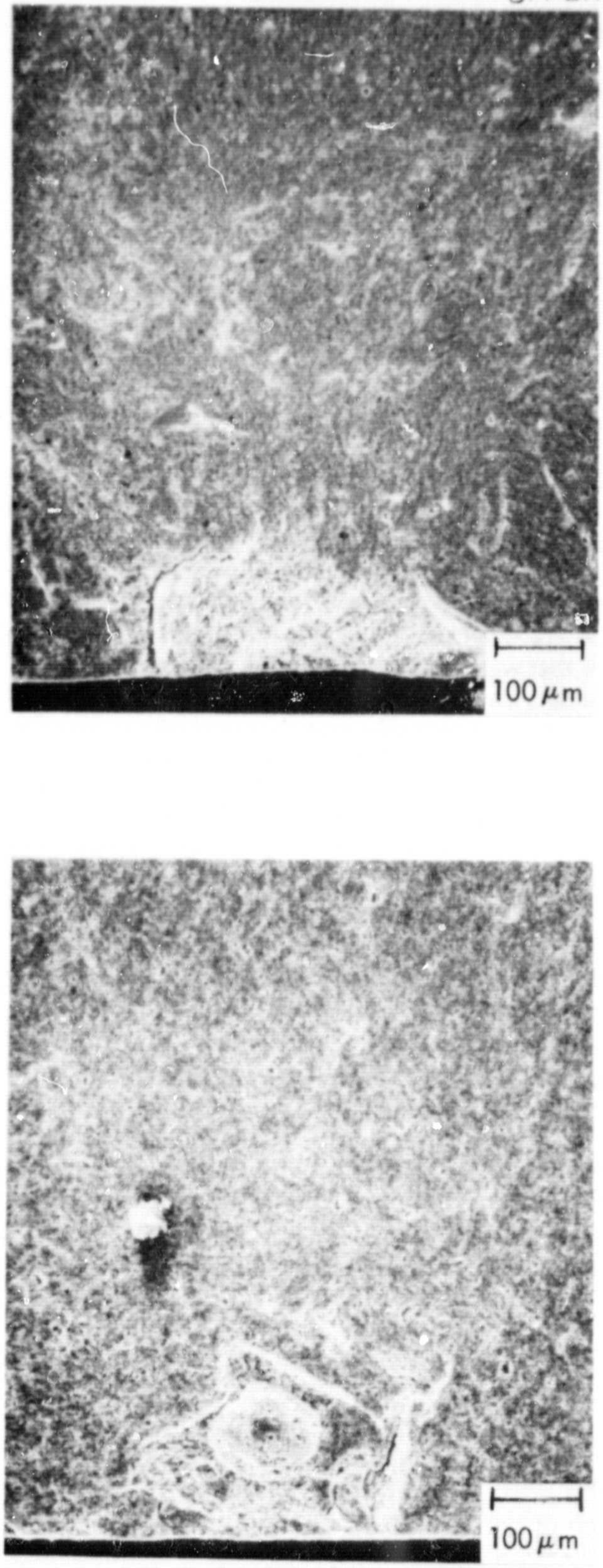

Figure 42. Fracture origins in (a) zircon and (b) zircon/alumina.

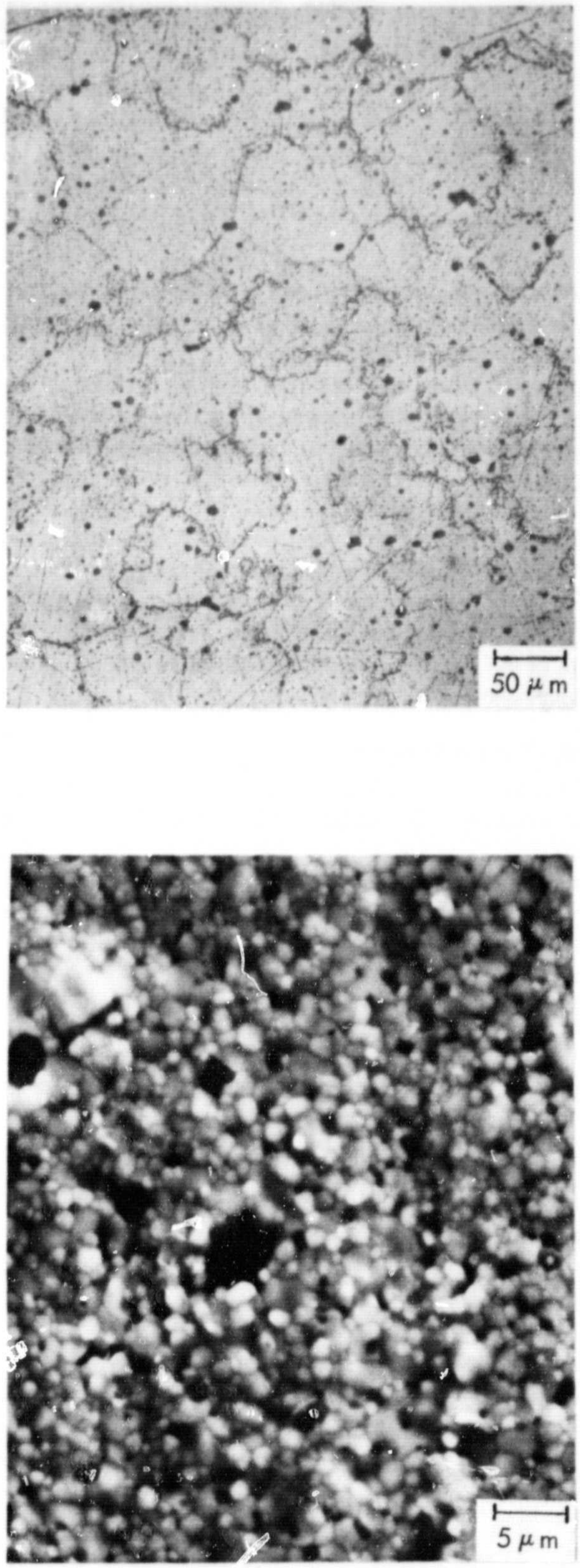

Figure 43. Microstructures for partially stabilized zirconia from (a) Feldmuhle International and (b) AC Spark Plug.

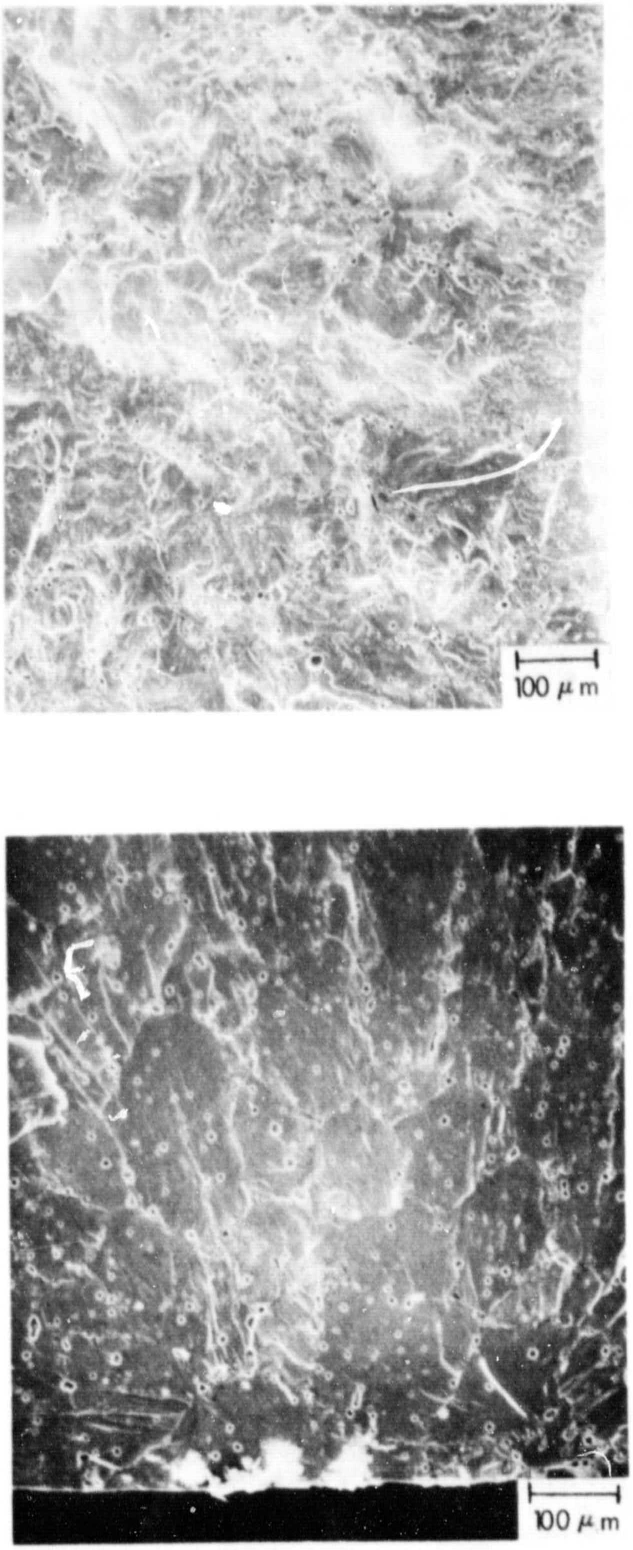

TE82-1135

Figure 44. Fracture surfaces for Kyocera International partially stabilized zirconia.

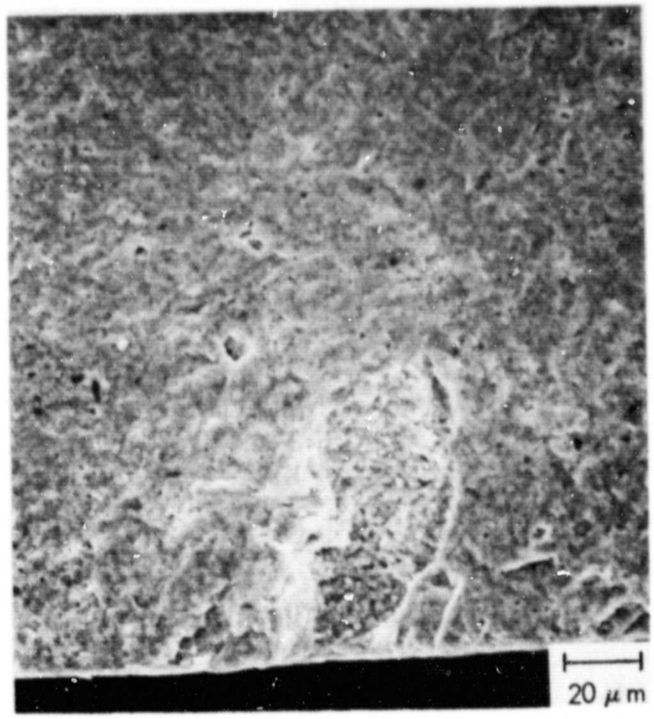

(a)

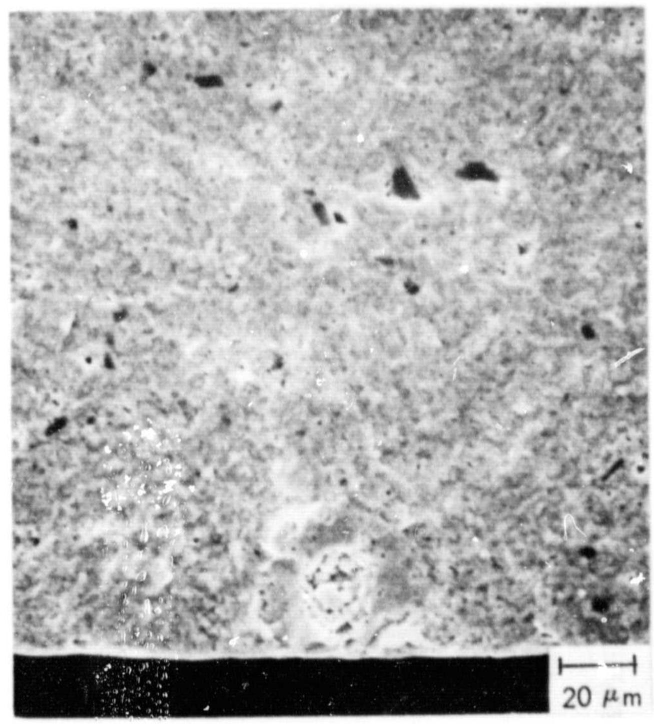

(b)

TE 82-1136

Figure 45. Strength controlling defects in AC Spark Plug partially stabilized zirconia.

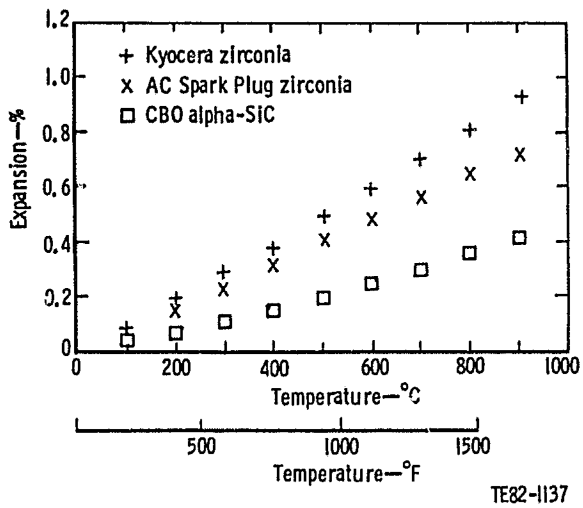

Figure 46. Expansion versus temperature of AC Spark Plug and Feldmuhle zirconias.

Table XI. Specific heat for AC Spark Plug and Feldmuhle zirconias.*

Temperature °C	°F	Specific heat—cal/g/°C
25	77	0.117
200	392	0.136
400	752	0.147
600	1112	0.154
800	1472	0.158
1000	1832	0.160

* Specific heat is identical for both companies.

In summary, the strength, expansion, and specific heat have been measured for two partially stabilized zirconia materials. Both materials have an average strength greater than 206.8 MPa at 1000°C (30.0 ksi at 1832°F). They differ slightly in that the AC Spark Plug zirconia expands 0.7% and Feldmuhle 0.95% between room temperature and 900°C (1652°F). Both materials have an equal specific heat of 0.16 cal/g/°C at 1000°C (1832°F).

9.2 Silicon Carbide Development

Development of reliable ceramic hot flow path components with emphasis on manufacturing technology is a major thrust of the AGT program. The Alpha Silicon Carbide Division of CBO has the primary responsibility for establishing the fabrication procedures needed to consistently produce ceramic components with the required dimensional and material property characteristics. The following subsections review and summarize the progress made toward this end during the current reporting period.

Gasifier Rotor

Considerable progress has been made in the development of the gasifier rotor as evidenced by spin tests. Silicon carbide rotors produced using injection molding have been most encouraging. In the last four lots of SASiC rotors, 76.9% have reached burst speeds in excess of 100% design speed.

Two lots of rotors were received for evaluation during this reporting period. They represent part of the output of an optimization matrix intended to increase the level of spin test burst speed. Variations in molding parameters, equipment, and composition are being addressed in this matrix. The two lots of rotors considered here differ in regard to the type of equipment used to form the green rotors.

Table XII. Density and nondestructive evaluations for injection molded rotors.

Lot No.	CBO No.	DDA No.	Density g/cm³	Nondestructive evaluations Visual	Zyglo	X-ray
6	296	FX24862	3.12	P*	P	P
6	297	FX24863	3.08	P	Porosity	P
6	303	FX24867	3.08	P	Porosity	P
7	404	FX24868	3.15	Chipped blade	Porous blades	Small pores in blades
7	410	FX24872	3.14	2 chipped blades	Porous blades	Small pores in blades
7	411	FX24873	3.14	P	Porous blades	Small pores in blades
7	412	FX24874	3.14	P	Porous blades	Small pores in blades
7	414	FX24876	3.09	Small chip	Porous blades	Small pores in blades

* P = passed inspection.

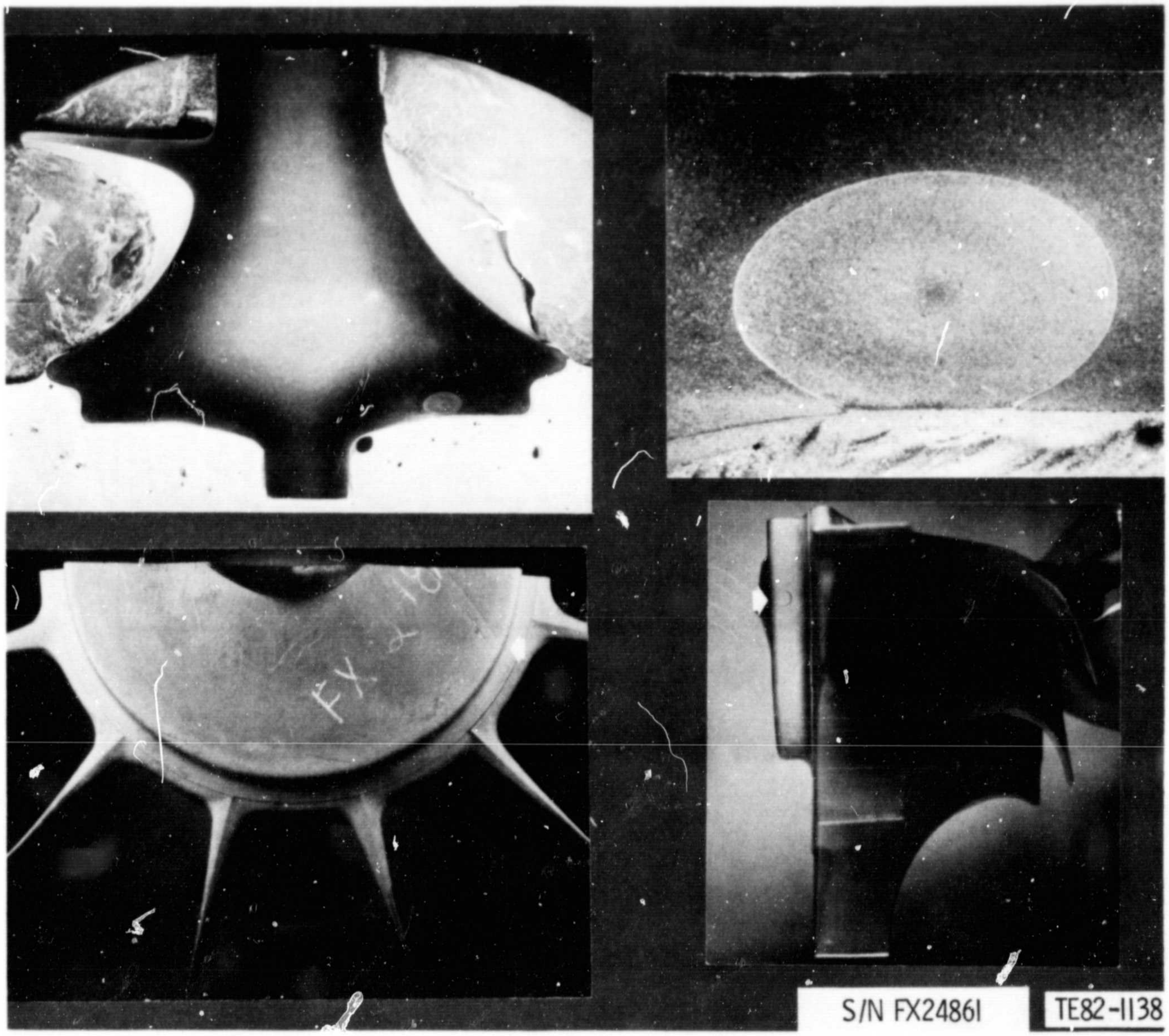

Figure 47. Defect in base of a Lot 6 rotor.

The results of nondestructive testing of Lots 6 and 7 rotors are presented in Table XII. While all the rotors passed a visual inspection, some differences were noted among those in each lot. In Lot 6 rotors there were some unique features on the base of several rotors. Figure 47 shows what appears to be a strand of injection-molded material. During the molding process some of the material apparently cooled when it hit the mold and remained as a strand of unsheared material. These indications were not observed in the Lot 7 rotors. In many cases these strands of material were associated with absorbed zyglo penetrant indicative of a crack or fissure of significant depth.

Figure 48 summarizes the spin test results for all rotors tested. Two of the three Lot 6 rotors tested (FX24863 and FX24862) failed at speeds below the 100% design level. Post test failure analyses showed that the fracture originated in both cases at the rotor backface. Figure 49 and 50, which show the primary fracture origins for both rotors, demonstrate that defects matching those described above precipitated failure. Corrective action to eliminate this type of defect has been initiated at CBO.

All Lot 7 rotors reached burst speeds in excess of the 100% level. The average speed for the five rotors tested was 94,800 rpm (110% of design speed). In most cases a fracture analysis was not possible due to the small size of the fragments. However, Figure 51 illustrates the fracture origin for rotor S/N 404 (FX24868). The origin was identified as a large subsurface pore. The corresponding schematic diagram shows the predicted stress at failure to be about 89.6-107.6 MPa (13-15.6 ksi) at the fracture

ORIGINAL PAGE
BLACK AND WHITE PHOTOGRAPH

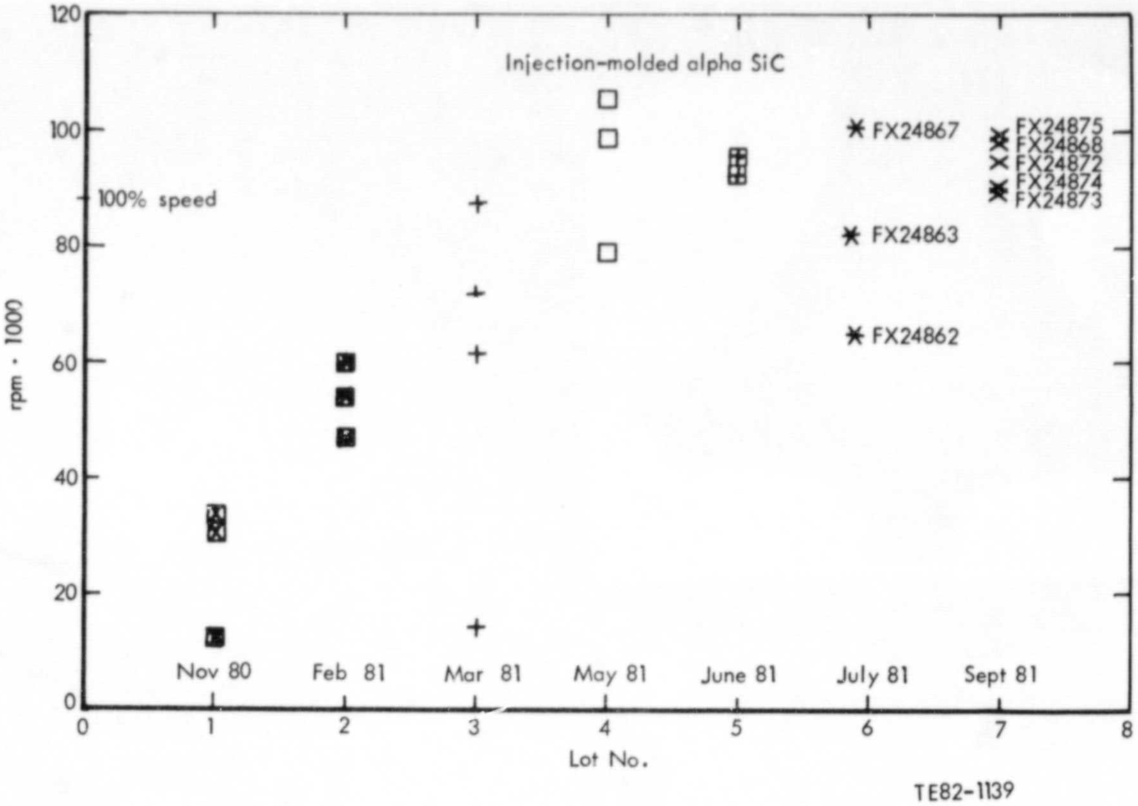

Figure 48. Burst test results for ceramic rotors.

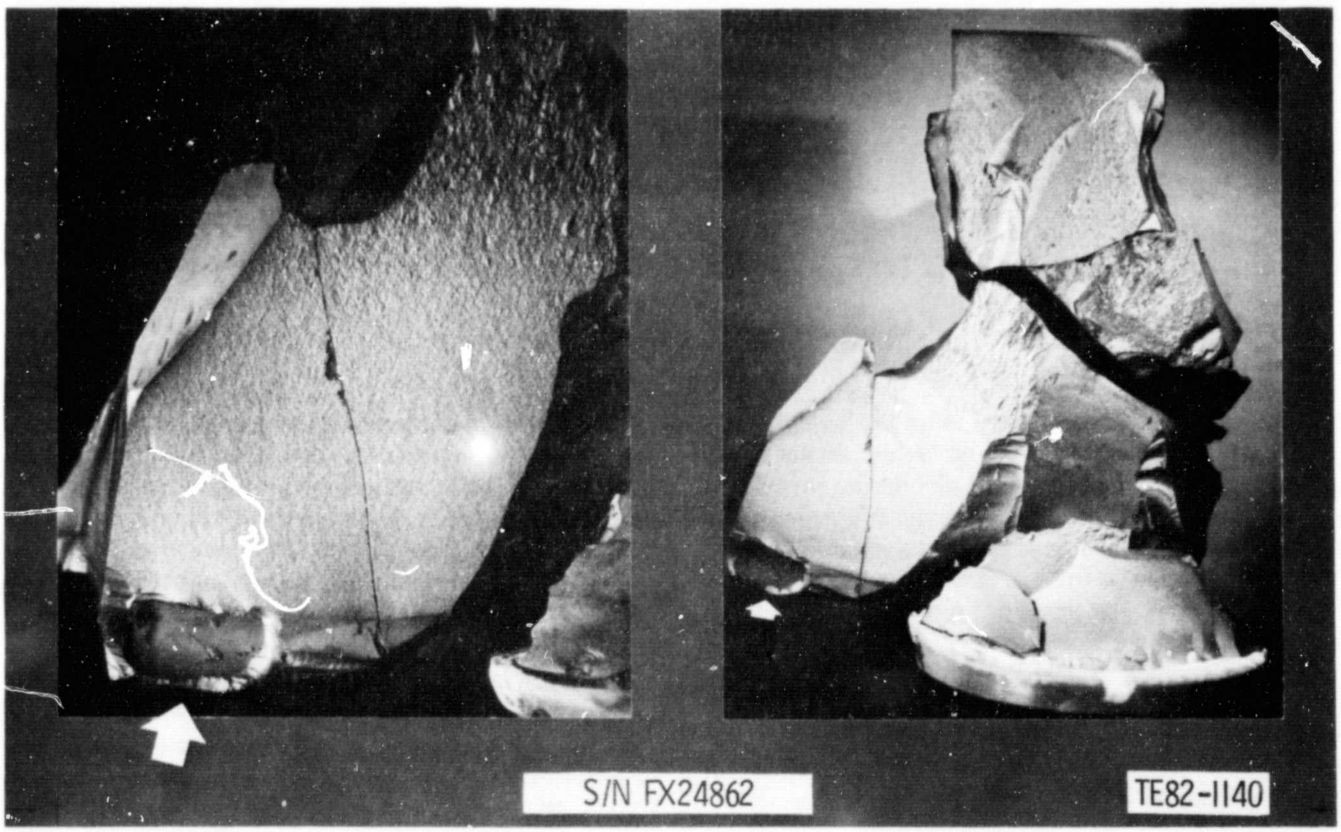

Figure 49. Defect in the base of a Lot 6 rotor initiated by burst.

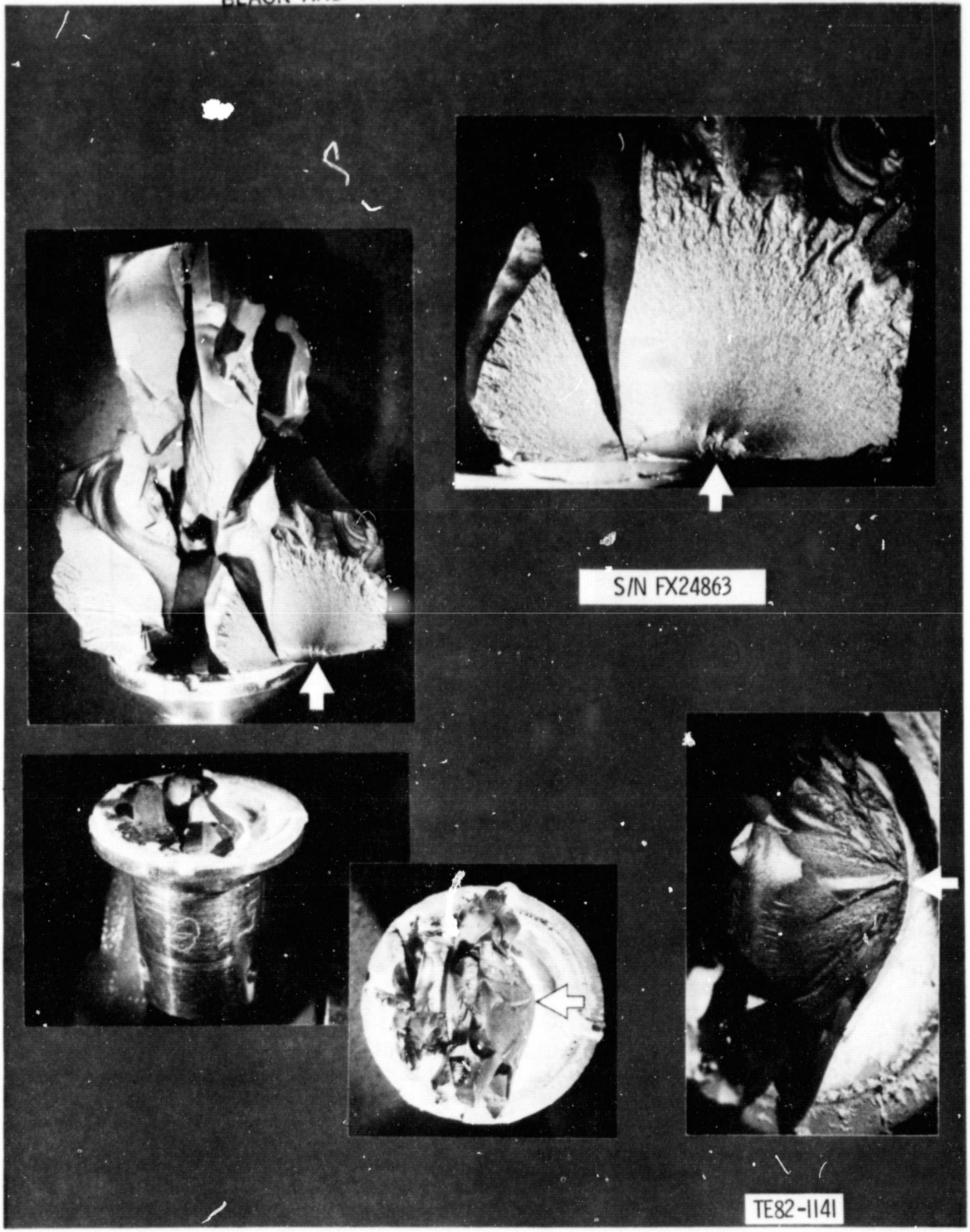

Figure 50. Fracture origin in the base of a Lot 6 rotor.

S/N 404
FX 24868

Failure speed—98,500 rpm

Fracture strength: 13.4 ksi
Calculated from fracture
mirror radius, +.

+—Location of failure origin

	MPa	ksi
A	0	0
B	13.79	2.6
C	35.85	5.2
D	53.78	7.8
E	71.70	10.4
F	89.63	13.0
G	107.56	15.6
H	125.48	18.2

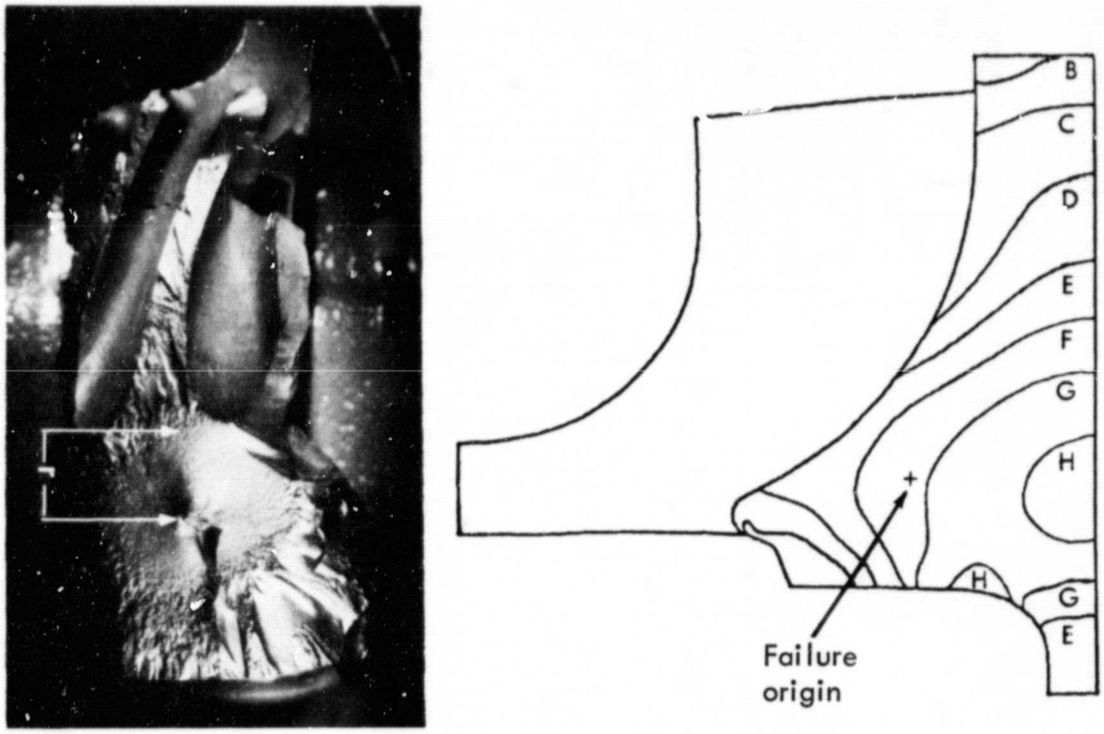

367540

TE82-1142

Figure 51. Internal fracture origin for a Lot 7 rotor.

origin. An independent analysis based on the fracture mirror size yielded a value of 92.4 MPa (13.4 ksi) at the instant of fracture, which is consistent with the result established by finite element analysis.

Combustor Assembly

COMBUSTOR BODY

During the past reporting period the combustor body was redesigned to accommodate repackaging in the AGT engine. Figure 52a illustrates the old combustor design and Figure 52b the new design. Eight combustor bodies of the latest design configuration have been sintered and inspected. Of the eight, two were found to be defect free. These two were found to be 0.51 mm (0.02 in.) and 0.76 mm (0.03 in.) oversize on their outside diameters but were acceptable. Some modifications have been made to improve the shrinkage reliability.

Strength qualification data for the combustor are given in Table XIII. Of the materials received for the combustor, the bimodal silicon carbide from CBO has yielded the highest strengths.

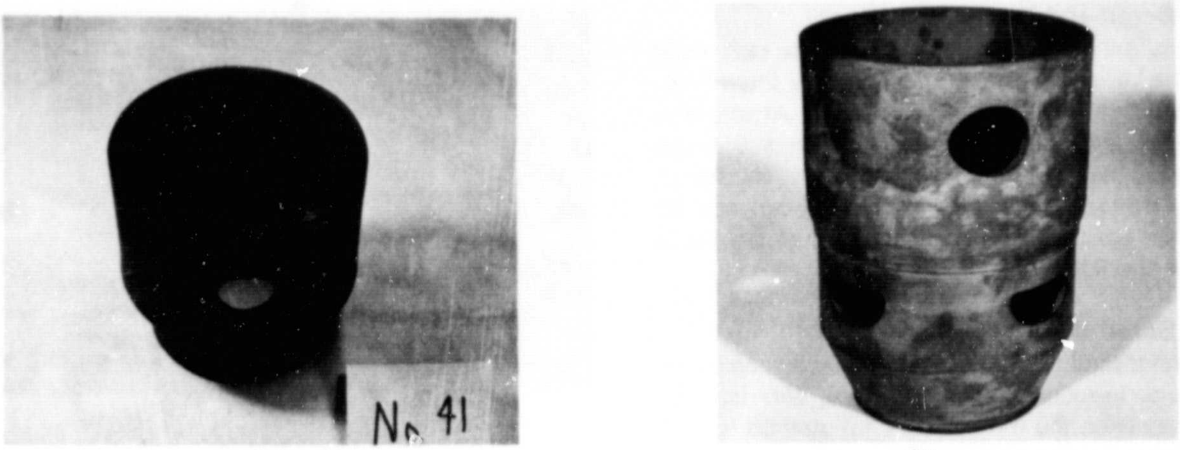

(a) (b)

TE81-5763A

Figure 52. Old design (a) and new design (b) of combustor body.

ASSOCIATED COMBUSTOR PARTS

Parts associated with the combustor body include the swirl plate, pilot tube, and dilution band. All of these components are being made from green machined isopressed silicon carbide.

Six swirl plates have been sintered during this period. Final machining of these parts is being performed by an outside vendor.

Six dilution bands and pilot tubes have been produced. Final grinding is expected to be finished by mid-February. Figure 53 shows a complete set of combustor parts.

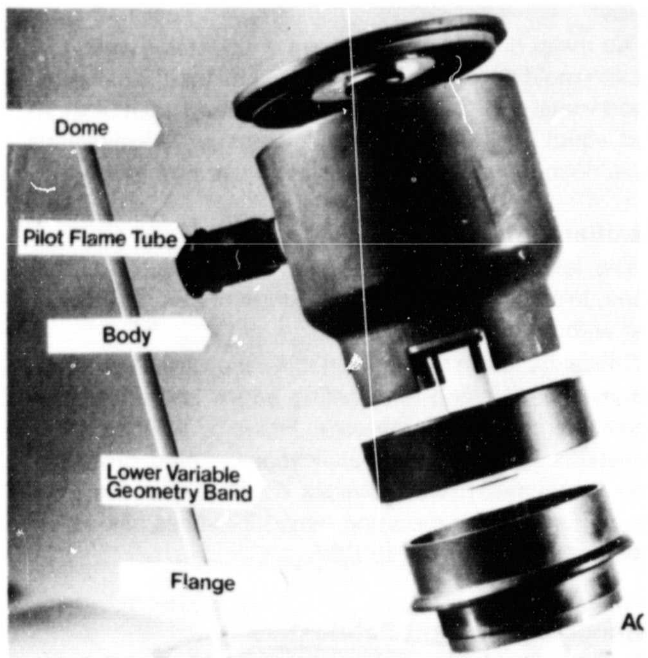

Figure 53. Combustor parts.

Table XIII. Strength qualification data for slip cast SASiC.

Tensile surface condition	Temperature	Average strength MPa	Average strength ksi	Weibull modulus	No. of Samples
As fired	Room temperature	334.9	48.58	5.3	20
Machined	Room temperature	411.5	59.68	7.6	10

Gasifier Scroll and Connecting Duct

Revisions are needed on the scroll slip cast mold design. The vane pocket region is presently three times thicker than the remainder of the casting. Attempts to add material after casting have not been successful. Modifications have been made to the scroll design. Models for making slip casting molds have been received for both the scroll and interconnecting duct (shown in Figures 54 and 55).

Gasifier Scroll Backplate

The gasifier scroll backplate has been fabricated by slip casting and injection molding (Figure 56). Injection molding has been the most successful method for producing thicker tab and vane pocket regions. The material used for this component has been SASiC.

Room temperature strength qualification data for the outer scroll backplate (10 samples, machined surface) was 309.81 MPa (44.94 ksi) with standard deviation of 27.30 MPa (3.96 ksi). The material density was 2.879 g/cm^3.

No major difficulties have been encountered during injection molding. Of the 39 compositions tried, 32 showed good visual quality. Four were sintered and each of these had about 1.59 mm (0.063 in.) warpage. Modifications have been made to try to alleviate these problems.

Gasifier Turbine Vanes

The last work on vanes involved evaluating dimensional tolerances after firing. Experiments were run with and without fixturing.

Critical factors in making suitable vanes are (1) distance between the leading and trailing edges and (2) dimensional integrity, i.e., no warpage. Figure 57 illustrates two deviations from design specifications. Some problems were encountered when cracks developed in the gate region. Early in this reporting period 31 vanes passed inspection and were sent to DDA.

Ceramic Component Fabricators

Components for the combustor assembly and thermal barrier applications have been manufactured by Kyocera International, Annawerk, and Pure Carbon. Strength qualification data have been received for these materials. The following subsections summarize the progress made to date for each of the above vendors.

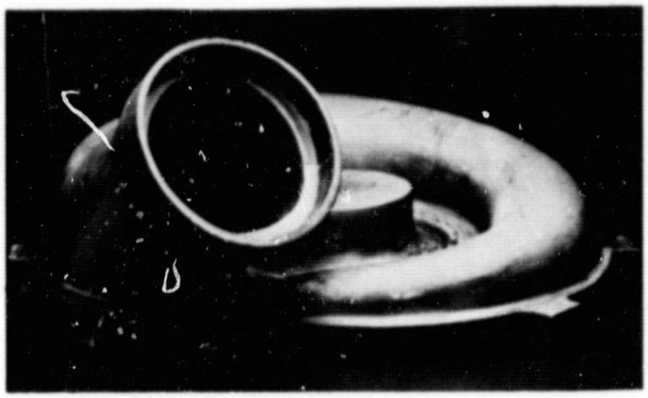

Figure 54. Gasifier scroll.

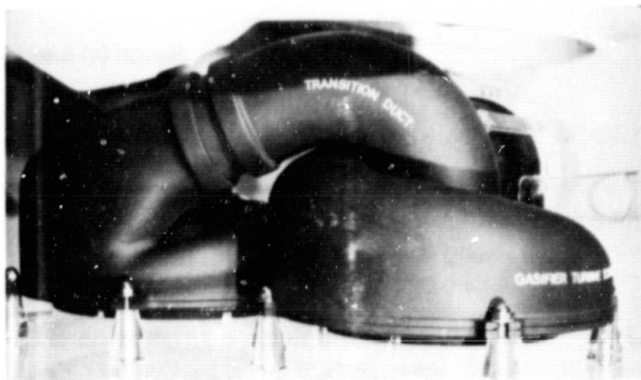

Figure 55. Interconnecting duct.

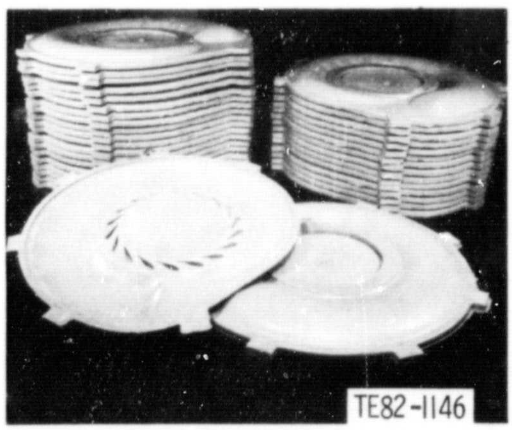

Figure 56. Injection-molded green gasifier scroll backplates, SASiC.

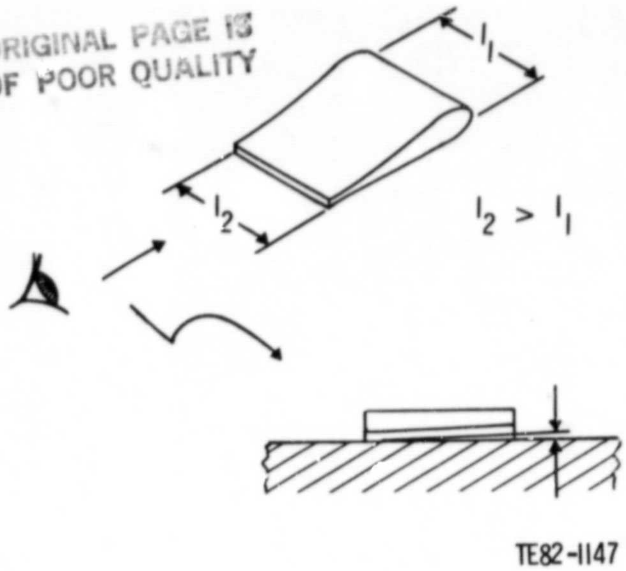

Figure 57. Vane distortion.

ANNAWERK COMPANY

Annawerk is making combustor bodies from slip cast RBSiC and sintered silicon carbide. Table XIV lists the strength qualification data received during this period.

PURE CARBON COMPANY

During this period strength qualification data (listed in Table XVI) were obtained for some extruded RBSiC. This material will be used for the flame holder component.

KYOCERA INTERNATIONAL

Kyocera has supplied the following silicon carbide components associated with the combustor assembly: dilution ring, flange, swirl plate, flame holder, and combustor body. Components have also been produced from isopressed zirconia for thermal barrier applications. Figure 58 shows all of the components received from all three of the above vendors.

Summary

A meeting was held to discuss the feasibility of supplying ceramic components for an accelerated engine build in March 1982. It was concluded that the combustor and its associated components, as well as the gasifier and power turbine vanes, can be delivered within the required time frame. CBO will fabricate rotors with a new tool prior to secondary shaft assembly. As discussed previously, the scroll assembly has a high degree of uncertainty; a metal assembly will be used in its place. After machining, the assembly of the connecting duct work would be accomplished at CBO.

Table XIV. Strength qualification data for the combustor body from Annawerk.

Material	Density—g/cm^3	Tensile surface condition	Temperature	Four-point bend strength MPa	Four-point bend strength ksi	Standard deviation MPa	Standard deviation ksi	No. of samples
RBSiC	3.075	As fired	Room temperature	199.30	28.91	17.43	2.53	10
	3.067	Machined	Room temperature	232.12	33.67	37.43	5.43	10
Sintered SiC	3.169	As fired	Room temperature	235.63	34.18	31.02	4.50	10
	3.074	Machined	Room temperature	297.61	43.17	62.11	9.02	10

Table XV. Strength qualification data for the flame holder from Pure Carbon Co.

Materials	Density—g/cm^3	Tensile surface condition	Temperature	Four-point bend strength MPa	Four-point bend strength ksi	Standard deviation MPa	Standard deviation ksi	No. of samples
Slip cast	3.066	As fired	Room temperature	265.62	38.53	22.12	3.21	5
Refel RBSiC	3.067	Machined	Room temperature	429.84	62.35	44.46	6.45	10

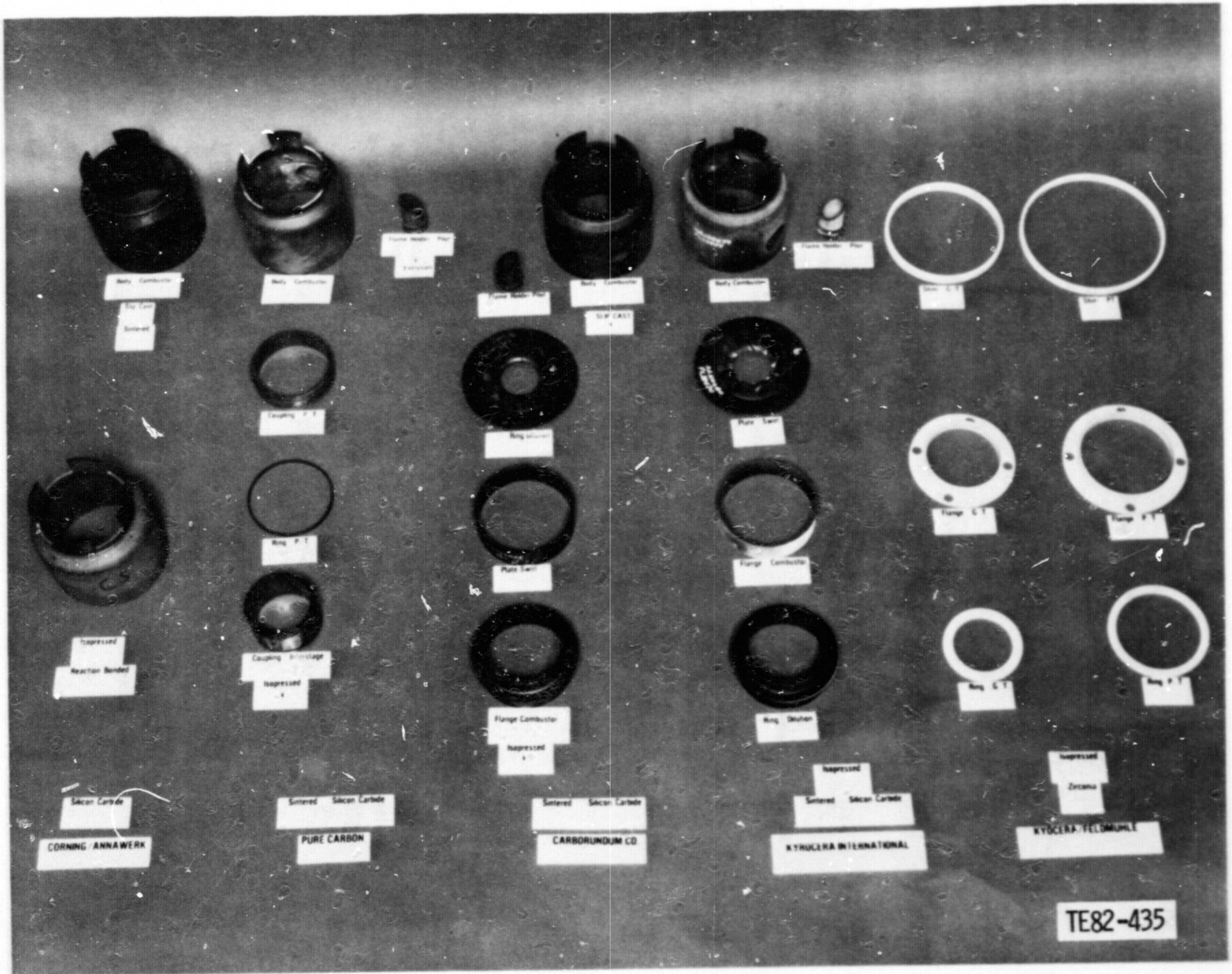

Figure 58. Silicon carbide components.

X. Controls Development

The controls effort over this period has been to design the electronic control system for the first scheduled dynamometer run. A preliminary electrical system has been designed and major components defined. The electronic control unit (ECU) to be used for this first test will be a modified digital control unit from another DDA program. All electronic boards designed from this existing unit have been built. The only modification is the addition of the required thermocouple channels. These additional boards have been designed but not built. The input/output pins have been assigned, and a preliminary schematic of all input/output devices has been developed. A relay panel has been designed to interface the ECU with the engine solenoids and ignition/starter.

The functions of a control console have been established, including the appropriate interface connections with the ECU. This control console will allow manual open loop control of gasifier speed, IGVs, burner variable geometry, and power transfer clutch. Switches, lights, and meters will also be provided to monitor the engine performance and to allow the control console operator to manipulate various engine conditions. Fuel flow is the only engine parameter that will utilize closed loop control, with which the amount of fuel flow is determined by the ECU software program and not manually set by an operator.

A preliminary schematic has been designed for an engine test simulator. All control console parameters will be included so that this unit can simulate all input/output to the ECU. Engine actuators, fuel valves, and thermocouples are represented as a static checkout only. Engine dynamics are not included, but the simulator can be used as a valuable tool to check out the control software logic for shutdown faults and proper sequencing during starts/shutdowns. This schematic has been completed and is being laid out.

The control software is being set up to be especially cautious and protective of the engine for this first dynamometer run while giving maximum flexibility to the control console operator. The overall control software logic has been developed with major modules, and their functions have been defined. Actual coding of the control software logic has begun with an existing in-house Motorola development system.

XII. Supportive Manufacturing, Cost, and Marketability

12.1 Manufacturing Feasibility

The manufacturing feasibility studies at Pontiac have been concentrated in two areas: (1) the engine component machining and assembly manufacturing engineering department and (2) the pressed metal manufacturing engineering department.

The analysis at Pontiac includes interaction with DDA resulting in design changes to improve manufacturing feasibility and/or to reduce cost. A significant amount of this type of activity occurred during the layout stage, with less interaction during the detail stage.

The status of the manufacturing feasibility and process analysis at Pontiac to date is as follows:

Location	Designs received	In process	Complete
Engine plant	58	25	7 (awaiting approval
Pressed metal	7	2	–

This activity is expected to accelerate during January and February to complete the first detailed cost estimate by March.

12.2 Cost Analysis

The Industrial Engineering Department at Pontiac is responsible for developing the total engine cost analysis. All component drawings and parts lists are channeled through this department, from which they are distributed to Purchasing or the various in-house manufacturing departments for manufacturing analysis and cost quotation. Finally, the Industrial Engineering Department will consolidate all of the cost data, which will then be furnished to the Finance Department for pricing.

The cost analysis effort for this phase of the program has been concentrated specifically on the engine, less controls. The status of work to date is as follows:

* Total parts/assemblies to be estimated	286
Drawings received	248
Parts purchased, finished, or in assembly	173
Make parts	66
Make or buy – to be decided	9
Drawings sent to Purchasing	62
Drawings sent to Manufacturing	65

* Includes all control system parts, many of which are not to be designed during this phase of the program but which will be estimated in comparison with spark ignition engine controls.

A problem has been experienced in finding sources for some parts, with seven returned to date as "no quote." These will require a further search for suppliers. Those parts for which a satisfactory quotation cannot be obtained from a supplier will, of necessity, be estimated by Pontiac to complete the engine cost estimate.

Purchasing has received quotations on 24 of the 62 parts queried to date. The remainder of the parts to be quoted will be sent out as the drawings are received from the Industrial Engineering Department.

Appendix A. Terms and Definitions

Symbol/Term	Definition
AGT	advanced gas turbine
AGT 100	the AGT model being developed by DDA
AS	aluminum silicate
BIT	burner inlet temperature
BOT	burner outlet temperature
Btu	British thermal unit
BU	build up
BVG	burner variable geometry
C	isenotropic spouting velocity $-2gJ\,\Delta h_{is}$
°C	degrees Celsius
CATE	a NASA/DOE development program "Ceramic Applications for Turbine Engines"
CBO	Carborundum Company
CDP	compressor discharge pressure
CGW	Corning Glass Works
CM	meridional chord
CO	carbon monoxide
corrected flow	flow $\sqrt{\Theta/\delta}$
CTE	coefficient thermal expansion
CY	calendar year
D_m	mean bearing diameter
DDA	Detroit Diesel Allison, Division of General Motors
DN	diameter of bore in mm x speed in rpm
DF-2	diesel fuel no. 2
DOE	US Department of Energy
EDR	Engineering Development Report (of DDA)
equivalent flow	flow $\sqrt{\theta_{cr}}\,\epsilon/\delta$
equivalent speed	speed/ $\sqrt{\theta_{cr}}$
equivalent work	$\Delta h/\theta_{cr}$
°F	degrees Fahrenheit
ft	foot
g	gravitational constant
GM	General Motors Corporation
GPSIM	general purpose simulation
GTE	General Telephone and Electronics Corp.
green matching	machining a ceramic before it is fired
h	enthalpy
h or hr	hour
hp	horsepower
Hz	Hertz (frequency)
i.d.	inside diameter
IGV	inlet guide vane
in.	inch
J	conversion factor, Btu to ft-lb, Joule
JP-5	jet propulsion fuel no. 5
kg	kilogram
km	kilometer
ksi	thousand pounds per square inch
L	liter
LAS	lithium aluminum silicate
lbm	pound mass
LCF	low cycle fatigue
M	mega—(one million)
m	meter
M-dist	meridional distance
mm	millimeter
Mod I	the first design of AGT 100 using some ceramic hot section components
Mod II	the second AGT 100 design with ceramic hot section
MOR	modulus of rupture
N	Newton, speed (rpm)
n	number of test samples
N1	gasifier speed of rotation
N2	power turbine speed of rotation
NASA	National Aeronautics and Space Administration
NDE	nondestructive evaluation
NO_x	oxides of nitrogen
o.d.	outside diameter
P	pressure
Pa	Pascal
PMD	Pontiac Motor Division of General Motors
Q	oil flow
°R	degrees Rankine
R_c	pressure ratio
R_θ	turbine expansion ratio
RBSiC	reaction-bonded silicon carbide
RPD	reference power-train design
S	standard deviation
s or sec	second
SASiC	sintered alpha silicon carbide
SLAM	scanning laser acoustic microscopy
SPAM	scanning photoacoustic spectroscopy
T	temperature
T_T	total temperature
T_{TI}	total temperature, inlet
T/C	thermocouple
thixotropic casting	casting enhanced by vibration to reduce viscosity of the cast fluid
THM 440-T4	designation for a GM transmission for X-body cars
TOT	turbine outlet temperature
T-S	total-to-static
T-T	total-to-total
U_T	rotor tip speed
V	viscosity

Appendix A. Terms and Definitions

Symbol/Term	Definition	Symbol/Term	Definition
VG	variable geometry	Δ	difference between two measurements, e.g., ΔT
W	Watt; bearing thrust load; mass flow	δ	pressure/pressure standard
W_c	cooling flow rate	Δh	specific work
WOT	wide open throttle	Δh_{is}	ideal specific work (total-to-static)
2-D	two-dimensional (analysis)	ϵ	$(0.740/\gamma)\,(\gamma+1/2)^{\gamma/\gamma-1)}$
3-D	three-dimensional (analysis)	η	efficiency
404	an industrial gas turbine engine by DDA	θ	temperature/temperature standard
505	an industrial gas turbine engine by DDA	θ_{cr}	$(V_{cr}/V_{cr}\text{std})^2$
γ	ratio of specific heats	$\bar{\sigma}$	average strength

References

1. "Advanced Gas Turbine (AGT) Power-Train System Development Third Semiannual Report," for work performed from 1 January 1981 through 30 June 1981, Detroit Diesel Allison EDR 10578, NASA CR-165504, December 1981.